

Emergence and Future of Exsolved Materials

Kalliopi Kousi,* Chenyang Tang, Ian S. Metcalfe,* and Dragos Neagu*

Supported nanoparticle systems have received increased attention over the last decades because of their potential for high activity levels when applied to chemical conversions, although, because of their nanoscale nature, they tend to exhibit problems with long-term durability. Over the last decade, the discovery of the so-called exsolution concept has addressed many of these challenges and opened many other opportunities to material design by providing a relatively simple, single-step, synthetic pathway to produce supported nanoparticles that combine high stability against agglomeration and poisoning with high activity across multiple areas of application. Here, the trends that define the development of the exsolution concept are reviewed in terms of design, functionality, tunability, and applicability. To support this, the number of studies dedicated to both fundamental and application-related studies, as well as the types of metallic nanoparticles and host or support lattices employed, are examined. Exciting future directions of research are also highlighted.

such a way to also ensure long term durability. Many different design approaches have generally been employed, nevertheless balancing the two major requirements of stability and activity has proven to be a difficult goal. For example, creating supported single metal atoms has been known to increase the activity of materials by several orders of magnitude^[1,2] but avoiding agglomeration remains challenging; core-shell particles allow for overall increased functionality, stability, and dispersibility^[3] while encapsulation methods, e.g., cages, protect the material from deactivation due to poisoning or sintering^[4] but require relatively complex synthetic procedures.

Over the last decade, a new approach to material design has been introduced, which provides a relatively simple, single-step, synthetic pathway to supported nanoparticles that combine high stability against

agglomeration and poisoning with high activity across multiple areas of application. This approach is now commonly known as redox exsolution.^[5] A schematic illustration of the process is given in **Figure 1**, and a timeline of key developments of the concept is shown in **Figure 2**. In this approach, the guest elements, which will later form the active sites, are usually substituted within a host oxide lattice (most often perovskite, ABO_3), and are released in the form of metallic nanoparticles at the surface after a thermal treatment, usually a reduction (Figure 1a,b).^[5] In its early stages of development, this was also referred to as solid phase crystallization or self-regeneration (Figure 2).^[6,7] The development timeline shows two periods of relative hiatus, between 1997 and 2002, and 2002–2013,^[8–10] followed by an abundance of studies and discoveries, ignited by work in 2013 showing that the exsolution process can be better controlled by using the defect chemistry of the host lattice (Figure 2).

This unique formation process, whereby the constituting atoms of the exsolved particles were initially a part of the support crystal lattice, results in numerous functionally useful properties revealed in recent years as highlighted via the timeline shown in Figure 2. One aspect is that there is a crystallographic alignment between the exsolved and host phases and that exsolved nanoparticles are partially embedded (“socketed”) in the support phase.^[11] This has proven to unlock many properties otherwise not possible with alternative methods. First, the exsolved nanoparticles are sintering resistant but also have the ability to redissolve into the lattice of the oxide support under an oxidative atmosphere. Such reversibility allows for regeneration of the materials through redox treatment, also alleviating agglomeration and enhancing the lifetime of the materials.^[12,13] Second, the socketing and alignment protects the nanoparticles


1. Introduction

Nanomaterials often provide high activity for a wide range of applications such as hydrocarbon catalysis, electrochemical conversion or photochemistry but usually require a compromise in terms of durability. Durability is, however, equally important in applications, especially in clean energy conversion technologies. Supported nanoparticle systems have received increased attention over the last decades because they have the potential to meet the activity levels required, although, because of their nanoscale nature, they need to be controllably constructed in

Dr. K. Kousi, Prof. I. S. Metcalfe
School of Engineering
Newcastle University
Newcastle upon Tyne NE1 7RU, UK
E-mail: kallio.kousi@newcastle.ac.uk; ian.metcalfe@newcastle.ac.uk

Dr. C. Tang
School of Engineering
Newcastle University
Newcastle upon Tyne NE1 7RU, UK

Dr. D. Neagu
Department of Process and Chemical Engineering
University of Strathclyde
Glasgow G1 1XL, UK
E-mail: dragos.neagu@strath.ac.uk

 The ORCID identification number(s) for the author(s) of this article can be found under <https://doi.org/10.1002/sml.202006479>.

© 2021 The Authors. Small published by Wiley-VCH GmbH. This is an open access article under the terms of the Creative Commons Attribution License, which permits use, distribution and reproduction in any medium, provided the original work is properly cited.

DOI: 10.1002/sml.202006479

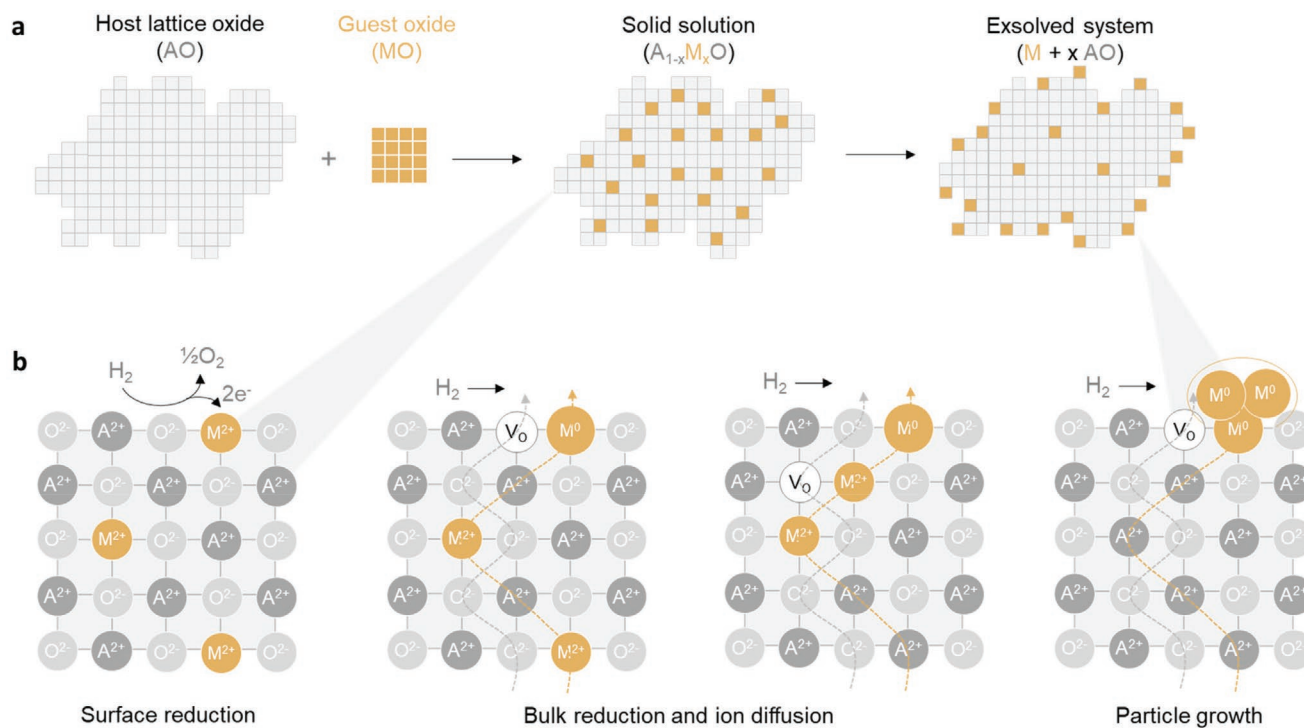


Figure 1. A schematic illustration of the process. a) The exsolution method and b) key processes fundamental to exsolution.

from poisoning mechanisms such as carbon deposition, making them overall more durable and stable under reaction conditions.^[11] Third, exsolved particles have been found to be more active than their deposited counterparts, which is mainly attributed to their confined, socketed nature that imposes strain upon the nanoparticles.^[14] This provides opportunities for further tuning of exsolved materials functionality through strain engineering, since strain has been shown to control multiple material properties including ion, electron and thermal transport, magnetic properties, and catalytic activity.^[15] Moreover,

in terms of preparation as compared to infiltration, exsolution can also be less wasteful in terms of precursor requirements; it occurs in a single step, as opposed to several, and thus can be more cost and time efficient. At the same time exsolution offers exceptional control over particle characteristics (size, population, and distribution), which allows for fine tuning of the activity and the selectivity of processes that employ exsolved materials.^[5,16]

Due to the combination of activity, durability, as well as compositional, structural, and functional tunability, the application of exsolved materials has proven to be

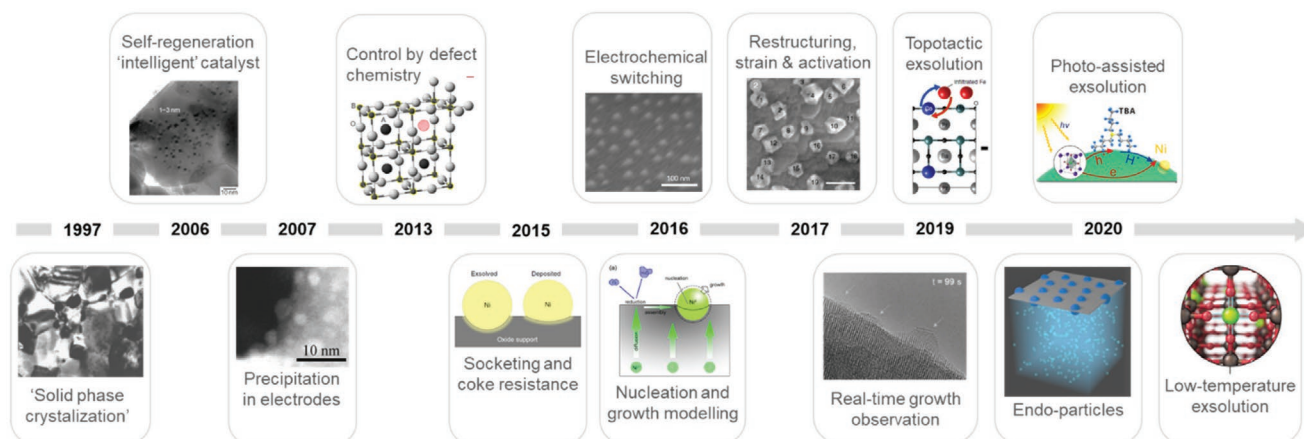


Figure 2. Timeline of key developments of the exsolution concept. Adapted with permission.^[5,8–11,15,16,22,23,26,40,125,140,157] Top row from left to right: Copyright 2006, Wiley-VCH, Copyright 2013, Springer Nature, Copyright 2016, Springer Nature, Copyright 2017, Springer Nature, Copyright 2010, Elsevier. Bottom row from left to right: Copyright 1997, Royal Society of Chemistry, Copyright 2007, Elsevier, Copyright 2015, Springer Nature, Copyright 2016, Elsevier, Copyright 2019, American Chemical Society, Copyright 2020, Wiley-VCH, Copyright 2020, Wiley-VCH.

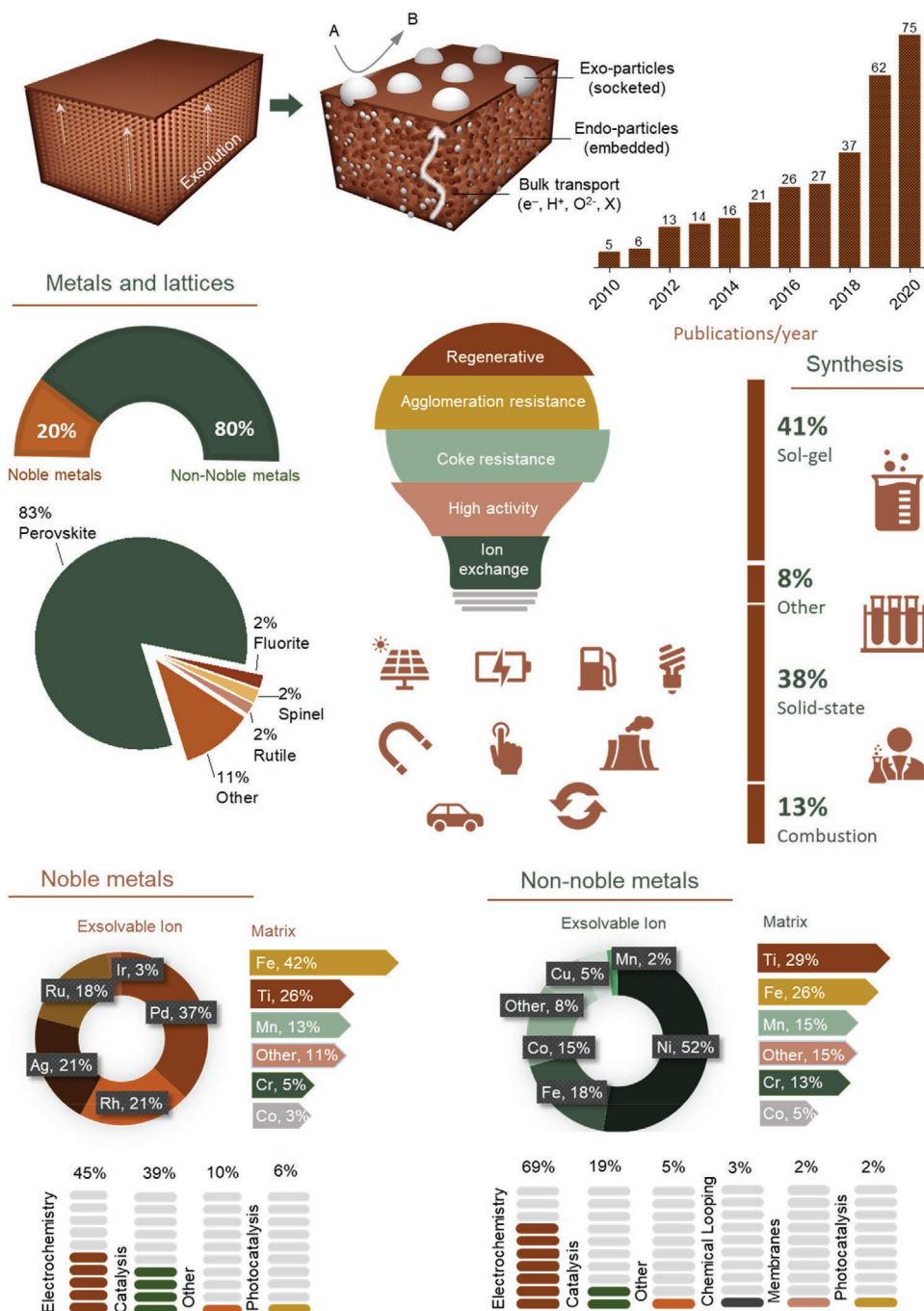


Figure 3. Exsolution infographic. Statistical analysis on a pool of 300 papers published on the field of exsolution since 2010.

game-changing across multiple fields including but not limited to energy conversion and storage and catalysis, as evidenced by more than 300 papers having been published since the first reports of the method a decade ago. However, to the best of our knowledge only four reviews covering different application-related aspects of exsolution have been published so far.^[17–20]

Here, we review the trends that define the development of the exsolution concept in terms of design, tunability, functionality, and applicability. We analyze a set of 300 papers published so far

on exsolution, to extract statistical information in terms of design elements (types of crystal structures, exsolvable and host lattice elements), synthesis routes, functionalities, and fields of application, including electrochemistry, catalysis photocatalysis, and other (discussed separately for noble and non-noble metal systems). The selected papers are listed and analyzed in the Supporting Information and the results are summarized in the infographic shown in **Figure 3** and in **Table 1** and based on these, we highlight exciting future directions of research in this fast-growing field.

Table 1. Areas of application of exsolved materials, including exsolved elements and B-site host lattice main element.

Application	Exsolved element	B-site host lattice	Refs.
Catalysis			
Methane conversion	Ni, Co, Rh, Ru, Ir	Mn, Ti, Ce, Fe, Mg	[96–100,125,134,141,147,148,155]
CO oxidation	Co, Ni, Pd, Rh, Ir	Co, Fe, Ti	[26,42,57,115,136,156]
NO _x conversion	Co, Ni–Co	Co, Ti	[26,135]
CO ₂ hydrogenation	Ni, Co, Rh, Ni–Rh	Al, Fe	[27,66,95,100,124,142]
Other	Ni, Co	Fe, Mn	[101,102,116,119]
Electrochemistry			
SOFC-air electrode	Ni, PrO _x , Co, Rh, Ag, Pd	Mn, Ti, Fe, Co	[69,71,120,133,152,153]
SOFC-fuel electrode	Ni, Co, MnO _x , Mo, Cu, Fe, Rh, Pd, Ru	Fe, Mo, Cr, Mn, Ti, Nb, Zr, Sc	[16,23,51,53,55,61,73–76,80,81,85,105,107,119,125,128,130,131,138,144,159]
SOEC/SOFC-symmetrical cells	Ni, Fe	Fe, Mn, Ti, Mo	[43,67,86,87,94,106,121,139]
SOEC-fuel electrode (steam electrolysis)	Ni, Fe, Cu, RuO ₂	Ti, Fe, Mo, V	[13,54,88–90,112–114,127,145]
SOEC-fuel electrode (CO ₂ electrolysis)	Ni, Ni–Fe, Fe, SrO	Ti, Mn, Mo, Ce	[77,78,91–93,108,111,132,160]
SOEC-fuel electrode (coelectrolysis)	Ni, Fe, Rh	Ti, Mo	[43,94,106]
Protonic ceramic cells	Ni, Ni–Co, Ru	Zr, Ti	[79,82,143]
Chemical looping			
Methane conversion	Ni, Ni–Co, Cu, Ni–Rh	Ti, Cr, Fe	[15,28,33,117,129,158]
Photocatalysis			
Water splitting	WS ₂ , Ag	Ti	[65,149,150]
Other			
Batteries	Co	Fe	[69,122]
Sensors	Ag, PdO	Fe, Nb	[137,151,154]
Oxygen transport membranes	Ni	Cr	[103]
Membrane reactors	Ni	Fe	[104]

2. Exsolution Fundamentals

2.1. Mechanistic Overview

In the exsolution method, illustrated schematically in Figure 1a, the active (i.e., exsolvable) elements are substituted in a host lattice under oxidizing conditions, forming an oxide solid solution, and released as metallic particles upon exposure to reducing conditions, leaving behind the host lattice as support. There are thus a number of key processes fundamental to exsolution, as schematically illustrated in Figure 1b: formation of a solid solution phase, exposure to reducing conditions to provide the driving force for the phase segregation, nucleation and growth of the exsolved phase, diffusion of ions, and oxide ions, and electrons across the host lattice to fuel the nucleation and growth process (generally shuttling between the bulk and the surface, but also locally if this occurs within the bulk or near-surface). Some of the key mechanistic steps are discussed below, while other aspects and specifics related to formation of solid solutions, driving forces, nucleation, growth, and diffusion are discussed throughout Sections 3.1–3.3.

Experimental evidence suggests that exsolution is, in essence, a phase decomposition process controlled by surface and bulk defects as well as external conditions.^[5,21–23] Metal cluster nucleation is typically favored at the surface where it is

facilitated by the presence of crystallographic defects that can act as nucleation sites, but it can also happen within the bulk in the case of host lattices that are easily reducible or that contain ions that are very reducible (e.g., noble metal ions).^[6,15] As the reduction progresses, more ions emerge at the surface to be reduced, forming additional clusters or growing existing ones.

The host lattice acts as a template for the nucleation of exsolved particles and as such, particles grow in an epitaxial relation with respect to the support (Figure 5a,b). The socketing of exsolved particles occurs in part due to contraction of the lattice due to loss of oxygen during reduction, and in part, due to evolution of the perovskite lattice around the nucleated particles.^[11,22] There are two studies that have attempted to elucidate the steps of socket–particle formation. One, provides evidence by atomic force microscopy that initially the nanoparticle nucleates in the subsurface, pulling the surface of the lattice inward to form a pit, from which the nanoparticle emerges in the later stages, resulting in the socketed interface.^[24] The second study is supported by environmental transmission electron microscopy (TEM)^[22] and shows the nanoparticles nucleating within the surface lattice, splitting and pushing the lattice laterally as the particle grows, to form the socket in a concerted manner rather than sequentially (Figure 4). The degree of immersion of the nanoparticles seems to also depend on the crystallographic

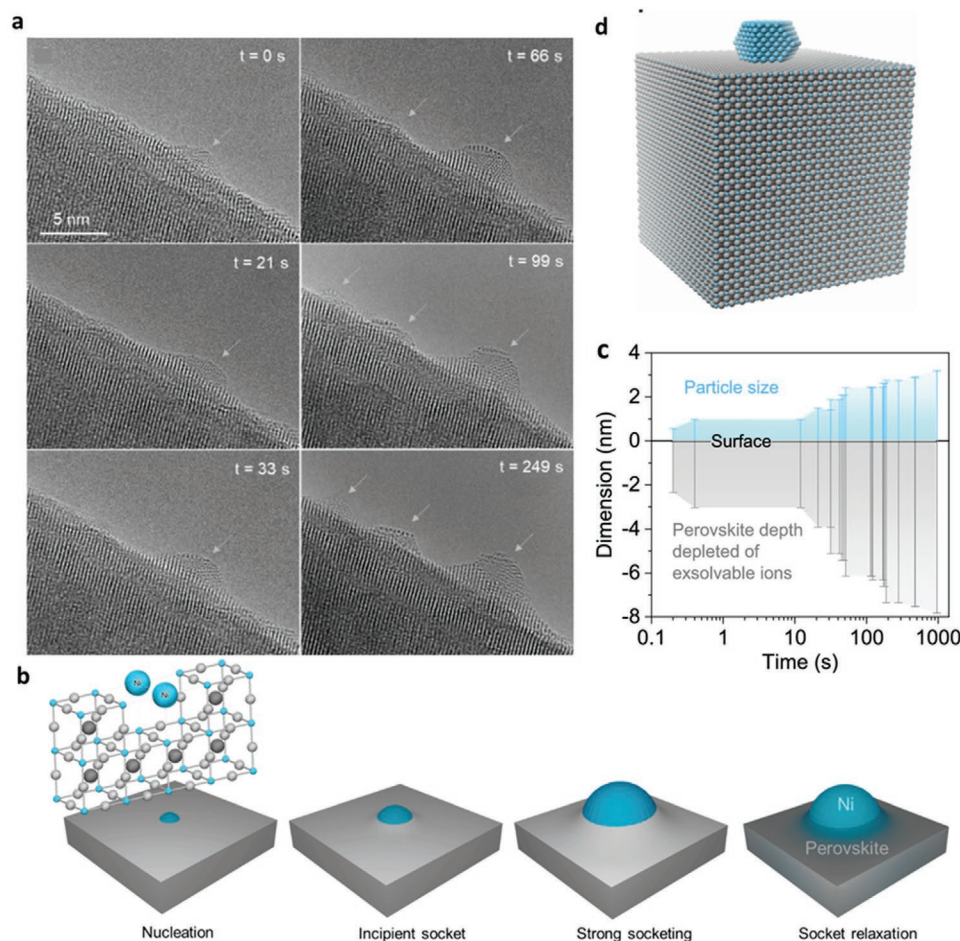


Figure 4. In situ observation of particle formation. a) Selected region followed throughout the exsolution process under H_2 showing snapshots at different times (t) of the gradual formation of a particle–socket and nucleation of two additional particles. b) Schematic illustration of particle–socket genesis during exsolution. c) Plot of the average particle size and corresponding depth within the perovskite that has been depleted of exsolvable ions. d) 3D model of a particle in final stages of growth and the corresponding perovskite volume required to form it. Adapted with permission.^[22] Copyright 2019, American Chemical Society.

orientation in which they nucleate.^[11] Nonetheless, the particles appear to grow in size proportionally in all directions and their growth versus time follows a quantized pattern. As evidenced by various models, the growth of the particles is largely controlled by an interplay between the diffusion of exsolvable ions, the strain under which the particle evolves in the socket and the (local) availability of exsolvable ions, with the latter two being the most prevalent.^[22,23]

2.2. Functionalities Unique to Exsolution

Due to the unique combination of fundamental processes through which exsolved particles form, they exhibit a unique set of functional capabilities, not found in systems prepared by conventional deposition methods. Some of these capabilities have been known for years and have enabled the use of these materials in a wealth of applications while others are only recently beginning to come to light. Most of these are highlighted through the development timeline shown in Figure 2.

Since segregation can, in principle, be reversed and thus the initial solid solution can be reformed, exsolution itself can be reversible, which was one of the first advantageous characteristics to be demonstrated (see timeline in Figure 2). Recently, it has been shown that reversibility in perovskite-based systems is largely controlled by A-site stoichiometry, which can lead to two different types of exsolution, reversible^[6,25] or irreversible.^[5] In the case of reversible exsolution, the parent perovskite matrix is stoichiometric and the metallic particles exsolve and redissolve in the said matrix by switching between reducing and oxidizing atmospheres, which leads to structurally flexible, dynamic structures. However, it has also been observed that after multiple redissolution cycles, the dissolution of particles back into perovskite becomes limited^[6] such that only metal clusters that formed within the bulk can redissolve, while the ones on the surface undergo coarsening instead.^[25] This could be due to the fact that surface oxidized particles are considerably larger than their counterparts in the reduced films.^[26] The ones in the bulk, on the other hand, seem not to be affected by this mechanism due to the slow diffusion of the metal ions in the bulk.

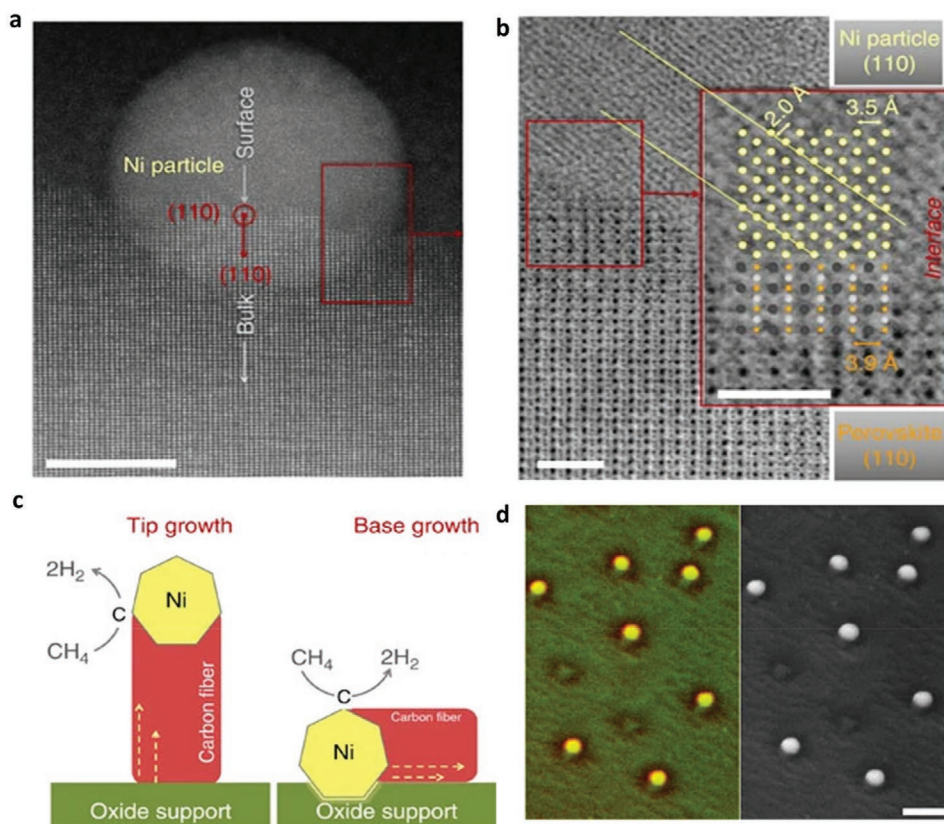


Figure 5. Alignment, socketing, and emergent anticoking properties of exsolved particles. a) TEM micrograph of a Ni particle exsolved on (110) native surface facet; scale bar: 10 nm. b) TEM micrograph detail of the metal–perovskite interface highlighting the corresponding atomic planes and orientations; scale bar: 1 nm. c) Schematic of possible carbon fiber growth mechanisms. d) False color and corresponding secondary electron micrographs of exsolved samples after testing under CH₄ atmosphere (green was used for the perovskite, red for carbon, and yellow for Ni metal). Adapted with permission.^[11] Copyright 2015, Springer Nature.

The socketed and epitaxial nature of exsolved particles with the parent perovskite enhance particle–substrate interactions (Figure 5a,b) allowing the materials to be protected against deactivation mechanisms, such as carbon deposition, leading to highly active, coke-free, sintering-resistant materials (Figure 5c,d).^[11,26] Moreover, this means that while exsolved particles are pinned to their initial locations, one can subject them to further chemical transformations to alter their composition, structure, and functionality, while preserving their initial spatial arrangement.^[26] At the same time, both the socketing and the crystallographic alignment induce strain into the particles, potentially leading to highly active samples.^[26,27] This is not surprising since appropriate control of strain has been proven to lead to increase in materials activity by several orders of magnitude.

Recently, a new dimension of exsolution has been demonstrated whereby materials with metallic nanoparticles dispersed throughout the bulk of oxide hosts were created (Figure 6). These materials have enhanced oxygen transport and exchange properties and demonstrate high activity and selectivity in catalytic transformations.^[15,28] By increasing the reduction temperature and the dwell time at reducing conditions, one could enable nucleation of particles in the bulk of the perovskite oxide. Due to the difference in crystal structure and unit cell

parameters between the particles and perovskite lattice, both phases become strained inducing bulk properties that have not been possible so far for these kinds of materials. This will be discussed in detail below.

Another important aspect of exsolution is its tailorability. As will be shown in Section 3.4, various particle characteristics including size, population, and even shape can be controlled by changing the time, temperature and driving force for the exsolution. Particles with different shapes (round, square, and triangular) can be formed enabling access to catalytically active facets while metal–metal oxide heterostructures on the surface and in the bulk can unlock new capabilities, e.g., in magnetism and ion transport (Figure 7).^[15,29,30] Additionally, these capabilities can be combined with various functionalities and microstructures provided by the parent lattice to design unique combinations of functional properties. This combination of functionalities leads to endless possibilities for formulation; a selection of these suggested in Section 9.

3. Design Principles

Based on the fundamental processes that occur during exsolution as discussed in Section 2.1 and illustrated schematically

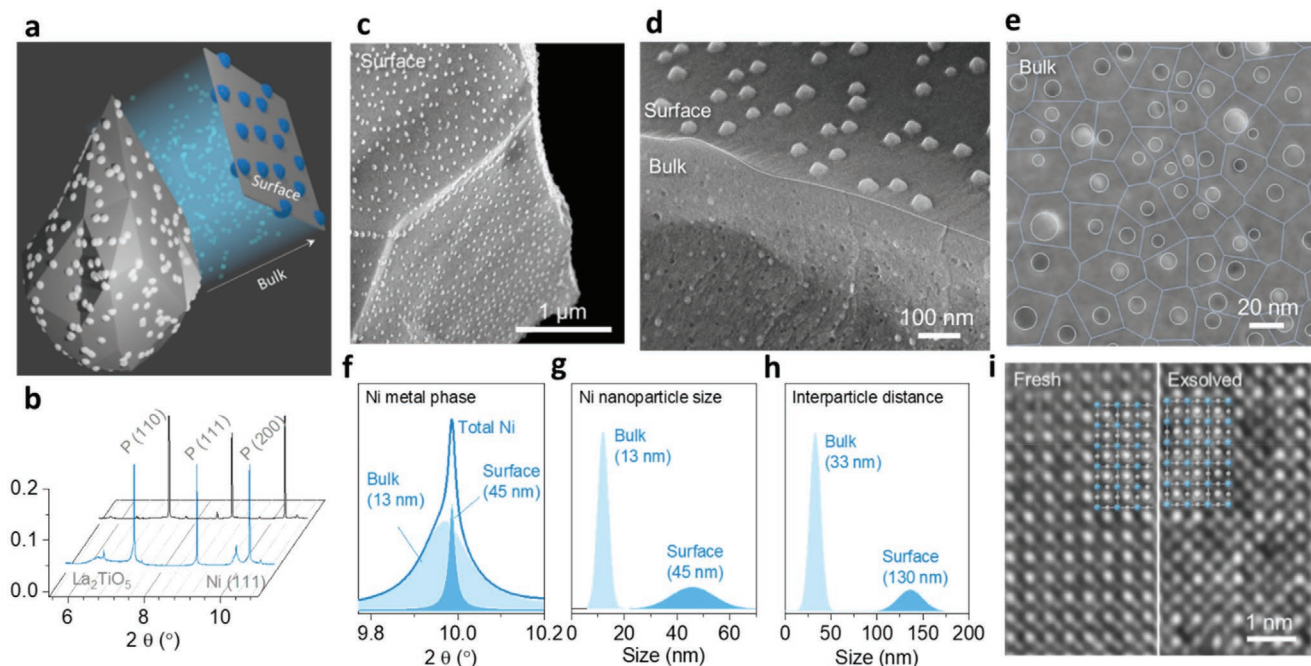


Figure 6. Creating systems with endo- and exoparticles. a) 3D model of a catalyst particle with nanoparticles dispersed on its surface and within its bulk. b) Room temperature XRD patterns in as-prepared state (black) and after exsolution at 1000 °C (10 h) in H₂ (blue). c,d) SEM micrographs showing an overview of the surface of the perovskite after exsolution and a cross-section view after exsolution revealing surface and bulk particles. e) Detail of the particles exsolved in the bulk. The micrograph is superimposed with a corresponding Voronoi tessellation highlighting a virtual partitioning of the perovskite bulk into nanodomains associated to each particle exsolved within it. f) Ni metal peak from panel (b) deconvoluted into surface and bulk particles contribution using Rietveld refinement. g) Ni metal particle size distribution of panel (d) calculated by image analysis. h) Domain size distribution calculated by image analysis on the Voronoi diagram in panel (e). i) TEM images of the perovskite lattice before (left) and after exsolution (right); superimposed are the lattice models. Reproduced with permission.^[15] Copyright 2020, Wiley-VCH.

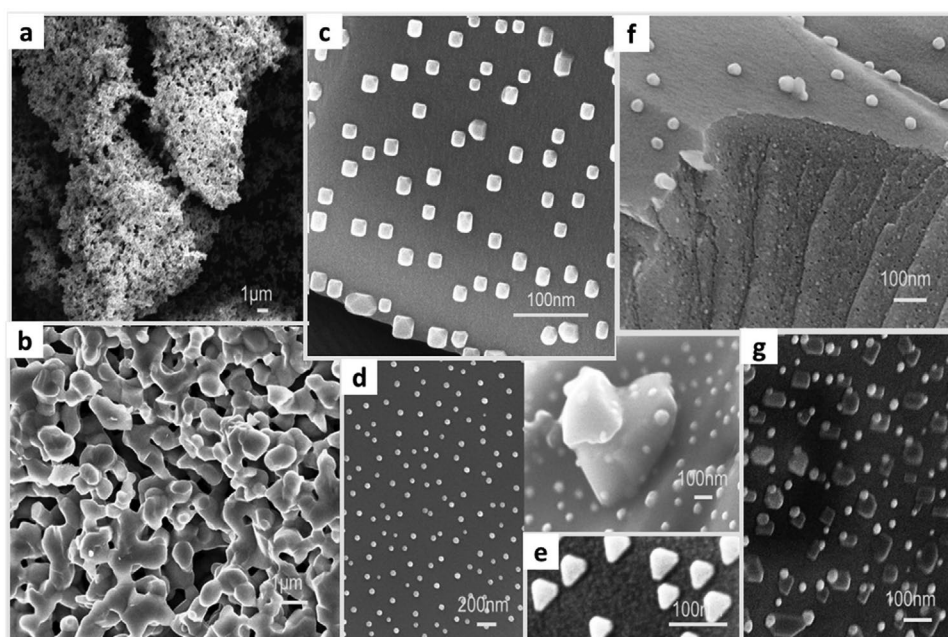


Figure 7. Opportunities in micro- and nanostructuring arising from the use of exsolution. a) Increased porosity in an oxygen carrier material. b) Porous electrodes for SOEC cells. c) Cubic metallic Ni particles. d) Round metallic Ni particles. e) Pyramid metallic Ni particles. f) A system with metallic endo- and exoparticles. g) Heterostructures consisting of ellipsoid-shaped particles interfaced with as-grown oxide phases.

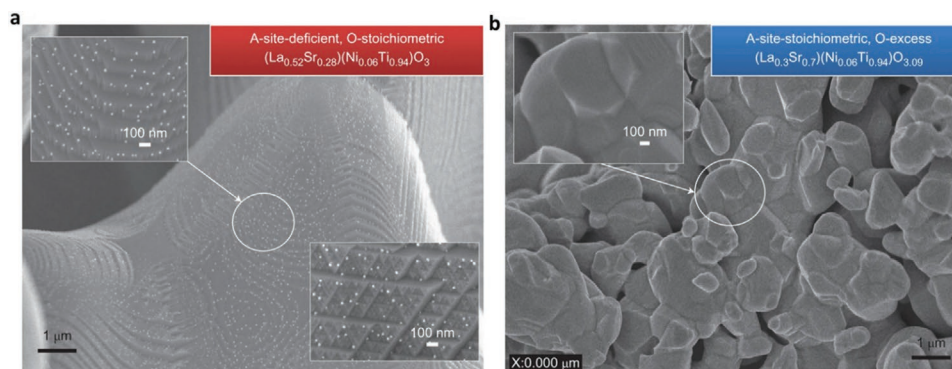


Figure 8. The role of nonstoichiometry in exsolution. Exsolution at the same conditions from a) an initially A-site-deficient, O-stoichiometric perovskite, and b) an A-site-stoichiometric, O-excess perovskite. Reproduced with permission.^[5] Copyright 2013, Springer Nature.

in Figure 1, multiple design elements need to be considered, including the type of host crystal lattice, the types of elements and corresponding ion size and reducibility, the lattice morphology, and extrinsic factors employed to trigger exsolution, as discussed below.

3.1. Crystal Lattices

Various crystal structures support, in principle, the formation of solid solutions, although not all solid solutions may support the other physicochemical processes required for exsolution, as outlined in Section 2.1. This is clearly reflected in the frequency with which certain crystal structures have been employed for exsolution, but also in the variety of resulting micro- and nanostructures. The most commonly used structure is the perovskite lattice, used by about 83% of studies from the 300 analyzed papers, while structures such as the spinels, fluorites, or simpler oxides (i.e., rutile) are more scarcely used, at about 2% for each of these.

The dominant role played by the perovskite structure is probably not surprising considering it is the more complex oxide in this list, which brings benefits but also limitations. For example, its relatively higher complexity means that the perovskite lattice natively supports mechanisms for concurrent cation, oxide ion, and electron transport (all key in the nucleation and growth of nanoparticles), to a much higher degree than spinel lattices (limited oxide ion and electron transport), fluorites (mostly oxide ion transport) or other simple oxides.^[31] On the other hand, spinel and simpler oxides are not composed of ions of vastly different sizes (as the A and B ions in the perovskite), do not generally exhibit a strong surface A-ion segregation as perovskites do, which generally hinders nucleation and exsolution.^[5,11] Additionally, due to their structure, perovskites can accommodate a significantly higher variety of cations of different size, coordination number, or charge as compared to the rest of the above-mentioned crystal structures. Indeed, perovskite oxides (ABO_3) allow for almost all the transition, noble and rare earth metals to be incorporated in the A- and/or B-sites making them exceptionally tailorable.^[32]

Additionally, different crystal lattices bring their own defect chemistry, which has been shown to be one of the most important factors that could allow one to control and adjust

materials to the desired application. In this case, perovskites hold another distinctive advantage supporting a wide range of point defects and related structures. In particular, A-site cations and A-site vacancies play a determining role in the bulk transport of B-site cations in the perovskite lattice and in surface nucleation, and hence toward B-site exsolution.^[11] Specifically, the presence of vacancies (either A-site or O-site) is of high importance when designing materials because they both enable ion diffusion and therefore the release of exsolvable ions on the surface (Figure 8).^[5]

3.2. Elements, Ion Size, and Reducibility

Another important aspect of exsolution design and tailorability clearly resides in the elements with which the crystal lattices are populated with, the resulting exsolved particles as well as the residual perovskite lattice. This dictates not only the possible chemistry of the system but also the additional functionality and reactivity it could support for a given application. In this aspect, perovskites are again the prime choice given the vast number of elements they can accommodate, including noble and rare earth metals at the A- and B-sites making them exceptionally tailorable.^[32] The size of the ions is crucial because it dictates on which of the two sites (A or B) the exsolvable ion can be substituted. In the perovskite structure usually ions with high coordination number and bigger size are suitable for the A-site, while the ones with coordination number up to sixfold and smaller ion size substitute on the B-site (Figure 9a). As such, the vast majority of elements of interest to be exsolved would substitute on the B-site of a perovskite with the exception of Ag perhaps due to its larger size. This is important when considering other functionalities. For example, electronic conduction in perovskites largely occurs through the B-site and thus substitutions could interfere with this process. Additionally, the stability of the perovskite lattice is also largely dictated by the B-site and employing certain elements such as Ti and Cr could enhance stability since these specific elements form strong bonds with oxygen in the coordination environment of the perovskite lattice. Generally noble metals are bigger than transition metals, which would potentially limit their successful substitution on the B-site.

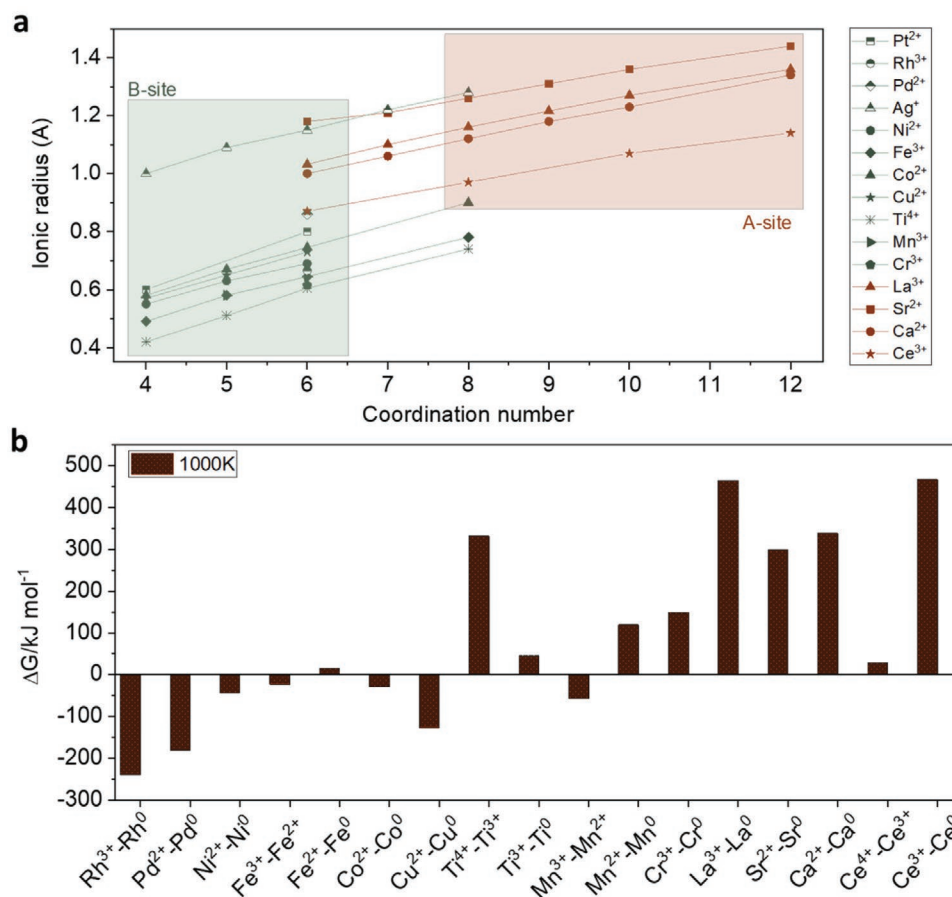


Figure 9. Design principles. a) Ionic radii versus coordination number for some ions usually encountered in perovskites. b) ΔG of reduction of different metal oxides.

While it is the overall lattice that needs to be reduced, the reducibility of individual constituting ions (or corresponding oxides) is important to consider in order to understand which ions could be exsolved selectively, thus which ones forming the nanoparticles and which ones remaining the parent lattice. Figure 9b shows a plot of ΔG of the reduction reaction of selected oxides. By comparison to Figure 9a, it is apparent essentially all A-site ions are not reducible to metallic state in typical conditions, and neither are certain B-site elements like Ti, Cr, Mn, etc. Thus it is generally the B-site ions that exsolve out of the lattice and are released on the oxide surface. For example, as confirmed experimentally, Ni substituted in a titanate will probably exsolve in large amounts at 1000 °C, while the Ti, originally on the B-site will still remain in an ionic state in the lattice of the perovskite even under these conditions.

While the A-site elements are not redox active or reducible, they still play a key, yet indirect, role in the exsolution process. Since the diffusion trajectory of B-site ions occurs through the A-site, the type of A-site ions (and defects) can interfere with exsolution.^[11] For example, La, Ca, or even Ce ions appear to be less fixed within their lattice positions than, e.g., Sr, allowing easier ion diffusion for exsolution and thus supporting particle growth.^[11] Taking into consideration the above, by designing a

perovskite that is A-site deficient and including an A-site ion that could facilitate the mobility of ions (e.g., Ca²⁺), one could make the rate determining process the oxygen rather than the B-site transport hence permitting a greater extent of exsolution.^[33] Additionally, the size of the A-site ions controls the tendency for surface A-site ion segregation, which in turn can affect both nanoparticle nucleation at the surface and ion transport through this segregated layer;^[5] for example, a strong correlation has been observed between the segregation energy of metals at the surface and the surface metal ion fraction. That is, preferential segregation of Ni toward the (100) TiO₂-terminated and (110) SrTiO-terminated surfaces in SrTiO₃ occurs due to the fact that these terminations appear to be have higher metal to oxygen atomic ratios.^[34]

3.3. Lattice Morphology

One of the most powerful aspects of exsolution is the possibility to trigger it on supports irrespective of their morphology, potentially facilitating material incorporation in devices and creating complex nano/microstructures. For example, exsolution can in principle occur from supports that are dense (outer surface and within bulk), porous (surface

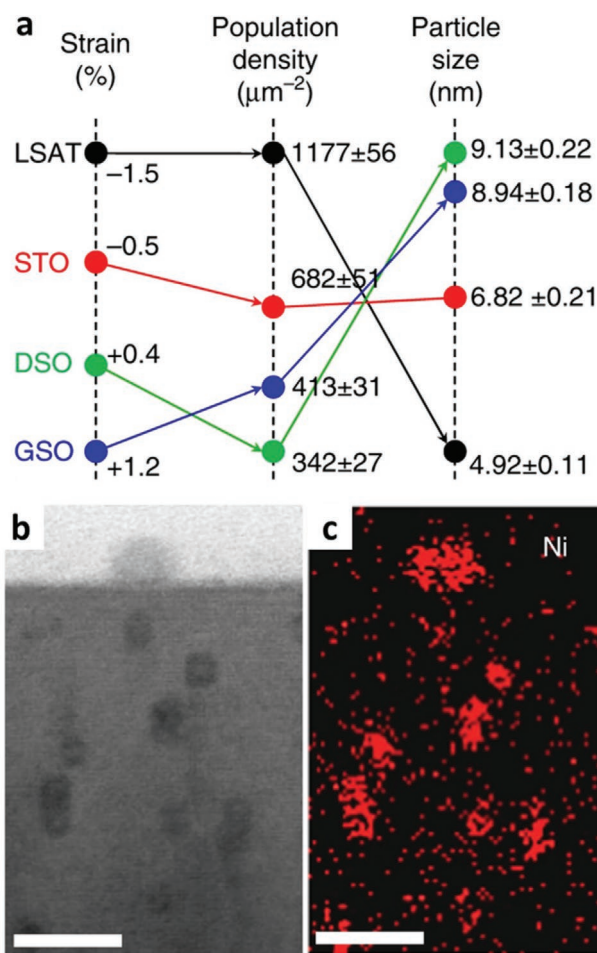


Figure 10. Exsolution in thin films. a) Effects of the substrate on three important physical parameters related to the exsolved thin films, strain, population density, and particle size. b) Ex situ cross-sectional STEM-HAADF image of the reduced thin film. c) EDS map of the image corresponding to panel (b). Adapted with permission.^[14] Copyright 2019, Springer Nature.

of inner pores and also potentially within bulk), in a loose powder (outer surface of the grains) or on thin films. However, changing the morphology of the support also changes the role of physicochemical processes fundamental to exsolution as explained in Section 2.1. For example, in high surface area powders or thin films surface nucleation would be more important than ion diffusion, since the distances the ions would be required to travel to the surface would be shorter. On the other hand, surface restructuring phenomena could be more prominent in these samples and thus could hinder exsolution. At the same time, aspects such as a high surface area, porosity and structural defects could promote exsolution at low temperatures.^[35]

While thin films are not quite as widely applicable as other sample morphologies, they have recently received more attention for exsolution applications due not only to theoretical reasons but also due to the fact that some of the microstructural challenges other systems pose can be avoided.^[36,37] For example, due to their length-scales on the order of tens of

nm, they potentially eliminate one of the three particle growth rate determining factors related to ion diffusion, leaving only the strain and availability of exsolvable ions. However, although simplified in a morphological sense, one can gain important insights into the design of materials by studying these model systems. For example, the type of strain the perovskite matrix is subjected to initially (which can typically only manifest on thin film length-scales) has been reported to affect exsolution characteristics immensely (Figure 10). More specifically, compressive strain leads to high particle population and small size while tensile strain leads to smaller particle population and larger size. In addition, microstructural strain is believed to enhance low temperature exsolution.^[14] One other important aspect revealed through studying exsolution on thin films is that the loading of the exsolvable ions on the B-site of a perovskite as well as the surface orientation of the matrix influences exsolution. Specifically, exsolution of (111)-oriented film produced the largest number of particles, the smallest particle size, the deepest embedment, and the smallest and most uniform interparticle distance among the oriented films.^[38]

3.4. Extrinsic Factors

Another powerful aspect of exsolution is the ease with which exsolution characteristics can be controlled. Various extrinsic parameters can be applied to a given solid solution in a set starting morphology of desired composition (i.e., intrinsic parameters) to create dramatically different final exsolved structures. The extrinsic parameters can be briefly summarized into the driving force for exsolution that is applied and the conditions, i.e., temperature and time, in which the reduction takes place. The driving force needed for exsolution to take place can be provided by either a reducing gas,^[22] an electrochemical force,^[16] or light.^[39,40] The most commonly encountered way to provoke exsolution is subjecting the materials to a high temperature reduction. This of course poses additional requirements as to the exact conditions as far as the oxygen partial pressure ($p\text{O}_2$) of the gas, the temperature of the reduction as well as the ramping rate to the required temperature.^[41] Depending on the materials studied it has been shown that high temperature leads to low particle population and larger particle size^[33,42,43] while one can have an impact on the nature of the exsolved species by changing the type of the reducing gas (Figure 11).^[22] For example, reduction under CO atmosphere could produce cubic particles while slightly humidified H_2 can lead to the exsolution of nanorods or even heterostructures.^[22,44] However, external conditions (temperature, $p\text{O}_2$) can cause a phase change in certain systems, which in turn can act as a driving force for particles to be released at the surface of the perovskite matrix. For example, it was observed that the phase change of a Co-doped $\text{Pr}_{0.5}\text{Ba}_{0.5}\text{MnO}_x$ double perovskite that takes place under reducing conditions induced the formation of a layered structure with ordered oxygen vacancies, further decreasing the oxygen coordination around Co sites and lowering the energy required for the Co/B-site cations to segregate and diffuse to the surface.^[45]

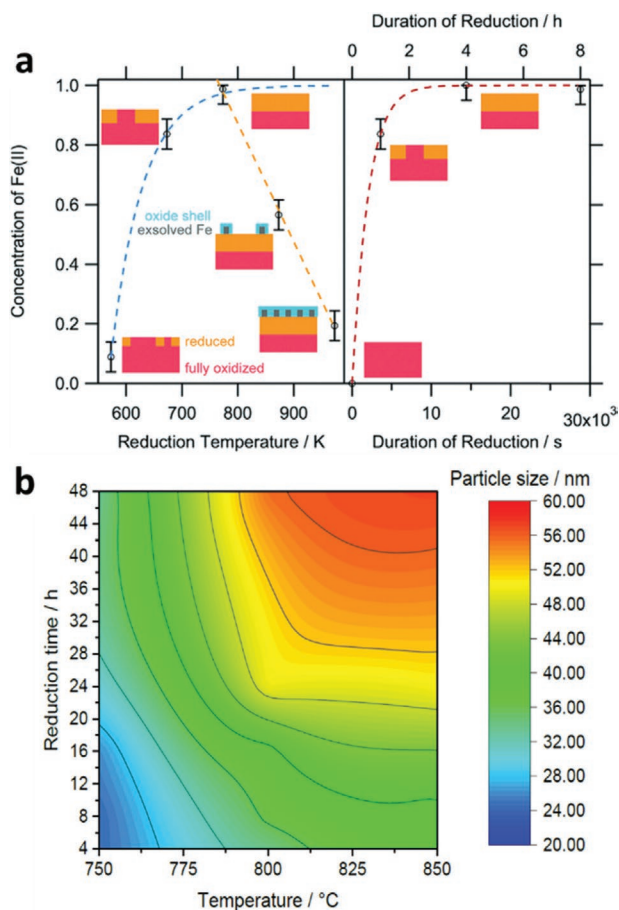


Figure 11. Exsolution control factors. a) Extent of Fe exsolution as a function of temperature and time. Blue-dashed line: limited growth model. Orange-dashed line: linear temperature-dependence of Fe^{2+} . Red-dashed line: Avrami-type fit model for the isothermal increase of the Fe^{2+} at 673 K reduction temperature. Adapted with permission.^[163] Copyright 2018, Royal Society of Chemistry. b) Particle size of exsolved Ni as a function of temperature and time. Adapted with permission.^[75] Copyright 2019, Wiley-VCH.

4. Modeling

While the experimental pool of evidence is relatively comprehensive, providing details on a great range of extrinsic and intrinsic factors that control exsolution, the corresponding modeling is almost entirely missing, as evidenced by the fact that only about 8% of the selected pool of papers are dedicated to or include modeling aspects. Given the complex processes involved during exsolution, one might have expected studies to attempt to model processes starting in the bulk of the material all the way to the interface and the particles themselves but there are actually only a few that do so (Figure 12). The studies that do exist have only touched on the impact of rather specific factors, failing to capture a complete picture of the process. As mentioned in Section 2.1, exsolution is largely governed by the strain under which particles grow as a result of being partly immersed, the diffusion of ions and the availability of exsolvable ions in the proximity of a nucleated particle. Modeling revealed, in agreement with experimental

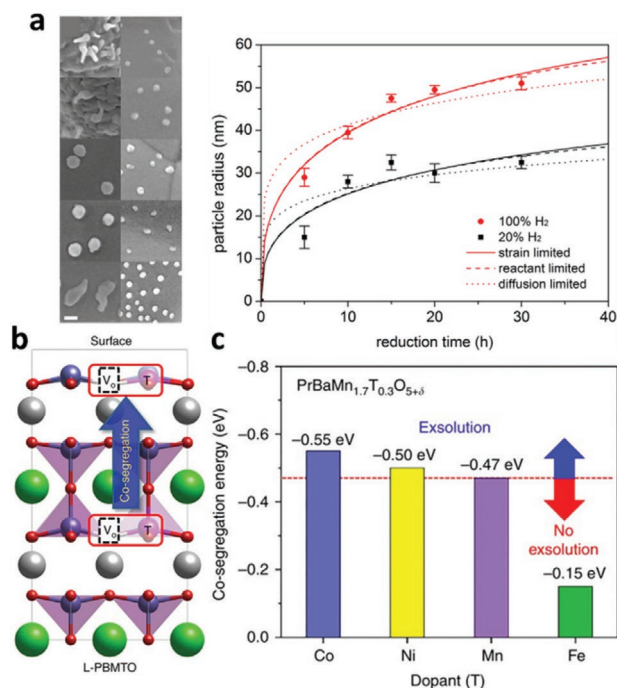


Figure 12. Modeling exsolution. a) Exsolution limiting models. Particles reduced in pure H_2 (left) and 20% H_2 (right) for 5, 10, 15, 20, and 30 h (from top to down) with the scale bar being 100 nm and the average particle size fitted with strain-limited model, reactant-limited model, and diffusion-limit model. Adapted with permission.^[23] Copyright 2016, Elsevier. b) DFT calculations from cosegregation energy. Schematic illustration of models used (Pr, Ba, Mn, T (Mn, Co, Ni, and Fe), and O atoms are shown as gray, green, dark blue, purple, and red, respectively), red boxes indicate the cosegregation of B-cation with an oxygen vacancy. c) Comparison of the cosegregation energy with the dopant (T) materials. Adapted with permission.^[61] Copyright 2017, Springer Nature.

results,^[22] that ion diffusion plays a minimal role (in perovskite systems that support ion transport) while the dominant factors that control exsolution are the concentration of exsolvable ions and the strain under which particles grow in the sockets.^[23]

One of the most modeled aspects is the role the oxygen vacancies play in the exsolution process. Most studies agree that they have a determining role in this process either because they seem to stabilize the segregated/exsolved phases^[7,46] or because they enable those phases to form.^[47,48] In particular, density functional theory (DFT) calculations supports the premise that the crystal reconstruction induces the loss of coordinated oxygen surrounding B-site cations, serving as the driving force for steering fast nanoparticle growth.^[45]

Another interesting aspect is the impact that the method of material preparation would have on the exsolution itself. Different preparation methods lead to materials with different grain size, crystallite size, and internal defects (which affect ion transport to the surface or could cause internal nucleation), as well as surface structure and composition (which affect particle nucleation and transport across the surface or near-surface regions and thus particle growth).^[21] It has been shown that the preparation method influences the pathway through which the particles exsolve because of the factors outlined above and

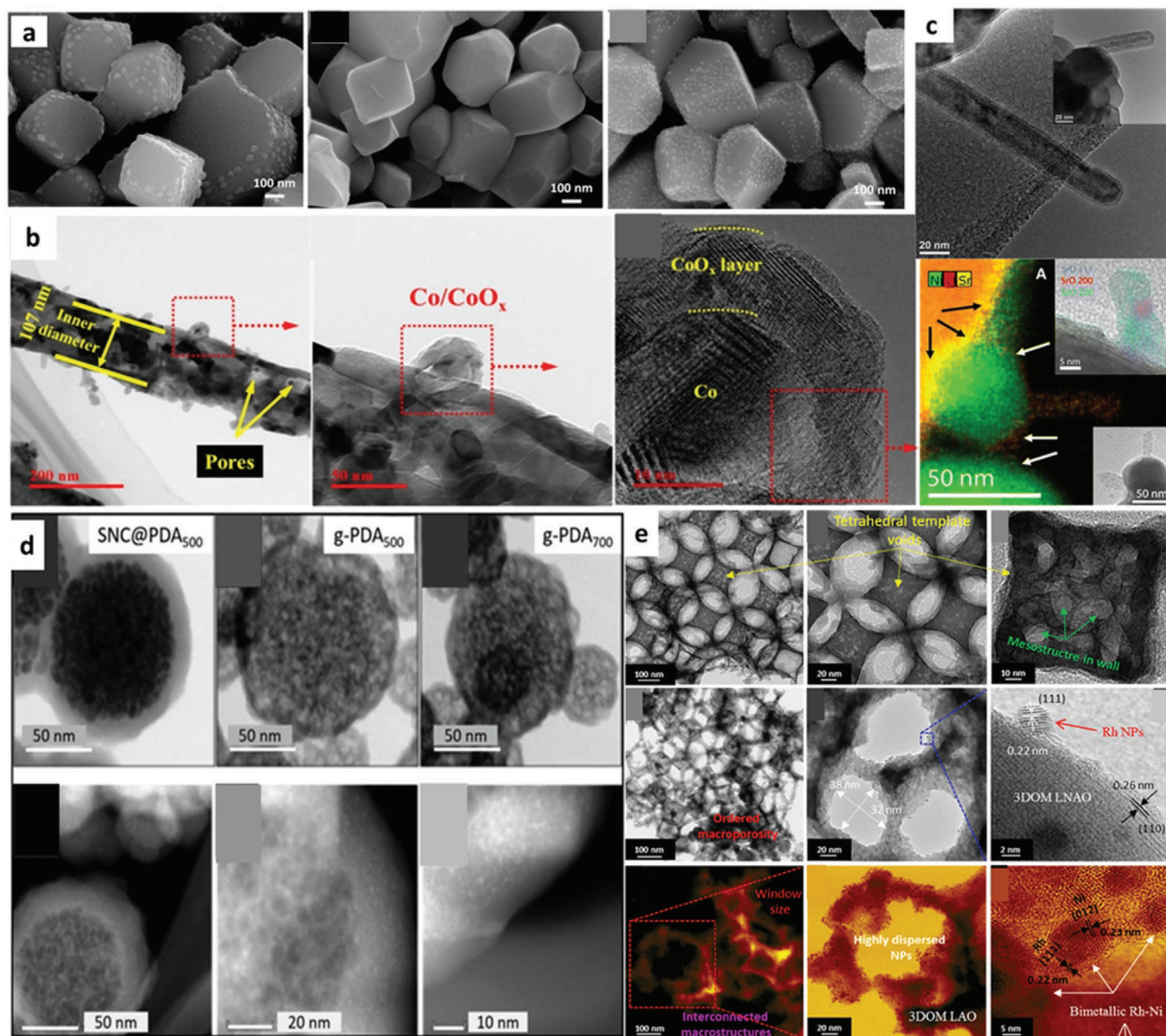


Figure 13. Exsolution from various microstructures. a) Ni supported NiO–MgO catalyst for methane steam reforming; SEM images of catalyst samples reduced, oxidized, and rereduced. Adapted with permission.^[97] Copyright 2018, Elsevier. b) Co exsolved porous nanotubular webs catalyst for soot efficient oxidation; bright-field TEM images and HRTEM images of Co/CoO_x on the electrospun nanofibers. Adapted with permission.^[116] Copyright 2019, Elsevier. c) Exsolution of Fe and SrO nanorods and nanoparticles from lanthanum strontium ferrite; TEM micrographs of LSF after exsolution highlighting the rod-like morphology of exsolved iron, and EDX maps and high-resolution HRTEM in the inset show the image of a single SrO rod (upper) and the image of a Ni particle with two attached SrO rods (lower). Adapted with permission.^[44] Copyright 2015, American Chemical Society. d) FeO_x NPs on N,O-doped carbon nanoshells for electrocatalytic oxygen reduction; TEM micrographs, FeO_x NPs are visible as brighter dots. Adapted with permission.^[109] Copyright 2019, American Chemical Society. e) Three-dimensionally ordered macroporous (3DOM) lanthanum aluminate perovskite catalyst with bimetallic Rh–Ni nanoalloys; HAADF-STEM images and EDS elemental mapping of as-prepared, Rh exsolved, and Rh–Ni exsolved samples. Adapted with permission.^[127] Copyright 2018, American Chemical Society.

the defects they introduce in the bulk lattice. In this case, those defects in the precursor phase influence the reduction pathway; facilitating the nucleation of Ni particles by acting as paths for enhanced diffusion or by lowering the activation energy required for nucleation, which DFT fails to model with results indicating very similar energies for all cases.^[21] This shows the need for theoretical studies to always be complemented with experiment to make sure such parameters are taken into account. A review paper published recently on computational

approaches to exsolution attempts to give an overview on this complex phenomenon stressing the importance in combining experimental and theoretical approaches.^[17]

Last, the nature of the exsolvable ions is an additional aspect, which many studies focus upon. These studies mostly concern reversible exsolution and noble metals. Exsolution reversibility or irreversibility is thought to depend on the ionic radii of the exsolvable ion as compared to the size of the unit cell of the host perovskite.^[7,49,50]

5. Synthesis Methods

The solid-state method is one of the most widely used synthesis method when preparing the host matrix for exsolution, accounting for about 38% of the pool of papers. In conventional solid-state routes, precursors of A- and B-site metal ions (normally oxides, carbonates, and nitrates) are mixed,^[23,32,51–53] and the mixtures are subjected to prolonged high-temperature treatments to form perovskite phases.^[11] This is generally preferred due to the fact that it allows strict control of stoichiometry, which is critical when attempting to prepare materials with large amount of point defects. However, due to the high reaction temperature required (>1200 °C), this method usually produces perovskites with large grain sizes (>1 μm).^[54,55] Efforts have been made to produce perovskites with smaller grain size in order to promote surface exsolution while still using this method because it provides high control over stoichiometry, but grains smaller than ≈500 nm^[33,42] are difficult to achieve. Materials used in catalytic applications usually have high surface area requirements hence solid state synthesis is not commonly used in order to prepare exsolved materials for catalytic applications (only 8% from all the catalysis papers published on exsolution).

Sol–gel is another prominent synthesis technique used (sol–gel synthesis was employed in 41% of the papers covered by this review), which allows for phase formation at temperatures as low as 700 °C hence producing much smaller grains (tens to hundreds of nanometers).^[56,57] Therefore, a variety of sol–gel routes, including the citrate-based^[35] EDTA/citrate-based,^[58,59] and Pechini methods,^[60,61] have been extensively employed to synthesize perovskites for both catalytic and electrochemical applications. Moreover, the combustion method is often used, where glycine,^[62] citric acid,^[63] or both^[64] are added in the solution of metal nitrate precursors as both complexing agents and fuel. Apart from these predominant methods, a small number of studies have also reported on the synthesis of perovskites via hydrothermal methods,^[65,66] freeze-drying precursor methods,^[67] or methods employing molten salts,^[68] all of which are able to produce much smaller particles as compared to the solid state method because of the lower temperature and shorter duration needed for phase formation.

It should be noted that some additional, interesting synthesis routes have also been employed to produce advanced architectures such as 3D ordered microporous materials or nanofibers (**Figure 13**). In order to produce perovskite nanofibers the electrospinning method was employed^[69,70] and 3D ordered macroporous La_{0.95}Ag_{0.05}FeO_{3–δ}^[71] and LaAl_{0.92}Ni_{0.08}O₃^[27] (**Figure 13e**) were synthesized by using poly(methyl methacrylate) microsphere colloidal crystal templates that were wetted with the metal precursor solutions and subsequently heat treated. Such structures are thought to enhance mass and ion movement during exsolution and so enable more exsolvable ions to reach the surface. Last, pulsed laser deposition (PLD) has been employed in order to prepare thin films for fundamental studies on exsolution.^[6,72]

6. Non-Noble Metal Systems and Their Applications

Non-noble metal exsolution is the most studied area of exsolution including about 80% of the published papers in the

last decade in a wide variety of applications. There are quite a few transition metals that have been studied for their ability to exsolve and the inherent properties this could generate. However, the majority of the literature focuses on nickel exsolution (51%) with iron (18%) and cobalt (16%) studies coming a close second and third. Others studies include copper and manganese exsolution as well as some more “exotic” cases such as PrO_x and WS₂ nanorods although such cases remain very scarce. The parent matrix from which they exsolve is however a bit more diverse in nature ranging from titanates and ferrites predominantly, as well as Mn- or Cr-based perovskites. Matrix choice depends mainly upon the application the materials are designed for but also the specific properties the researchers attempt to enhance. For example, titanates exhibit more stability as backbone structures but require high temperatures in order to form, which could result in large grain sizes and limitations as to the exsolvable ions incorporated. On the other hand, ferrites have higher ion mobility and form at lower temperatures, which could in turn enhance exsolution. Manganates and ferrites are also more redox active, usually resulting in high oxygen capacity that is preferable for applications such as chemical looping (CL) but can be less stable than their titanate counterparts. Nevertheless, the areas of application are diverse but, electrochemical applications are most common (72%) with catalytic applications (16%) coming second, these mainly involving hydrocarbon transformation to H₂ and syngas.

6.1. Nickel

Ni stands out as the most commonly used metal across a range of applications from electrocatalysis, catalysis, to chemical looping and membranes. The extensive variety of applications seems to have been fuelled by exsolved Ni systems being consistently reported to exhibit higher activity and durability than corresponding systems previously prepared by deposition. In spite of the extensive investigations on the application of this metal, there are considerable discrepancies in the way activity or durability are benchmarked and compared, as well as the correlation of activity with various material chemistry or chemical engineering aspects.

In electrochemical applications, Ni has been used for solid oxide fuel cells (SOFCs),^[23,53,73–76] steam or CO₂ electrolysis cells^[13,77,78] or protonic ceramic fuel cells (PCFCs).^[79] Solid oxide fuel cells^[51,67] and in particular the anode electrode^[61,80–82] have been the most extensively researched areas of exsolution (**Figure 14b,d**). One of the initial challenges of applying Ni exsolution in SOFCs was related to ensuring sufficient degree of exsolution, hence several studies focused on maximizing this by exploring the use of A-site deficient perovskite anodes in comparison to stoichiometric ones. Generally it was found that A-site deficiency can have a major role in enhancing electrochemical properties by increasing the degree of exsolution^[83,84] or to a larger number of nickel particles on the surface.^[12] The effect of the nonexsolvable ion and its fraction on the B-site was also studied and it was demonstrated that the even partial replacement of Fe³⁺ on the B-site with cations that enhance perovskite lattice stability, such as Mg²⁺/Ti⁴⁺, increases the structural stability but decreases the electric conductivity under fuel conditions (e.g., in the presence of ethanol, methanol).^[55,85]

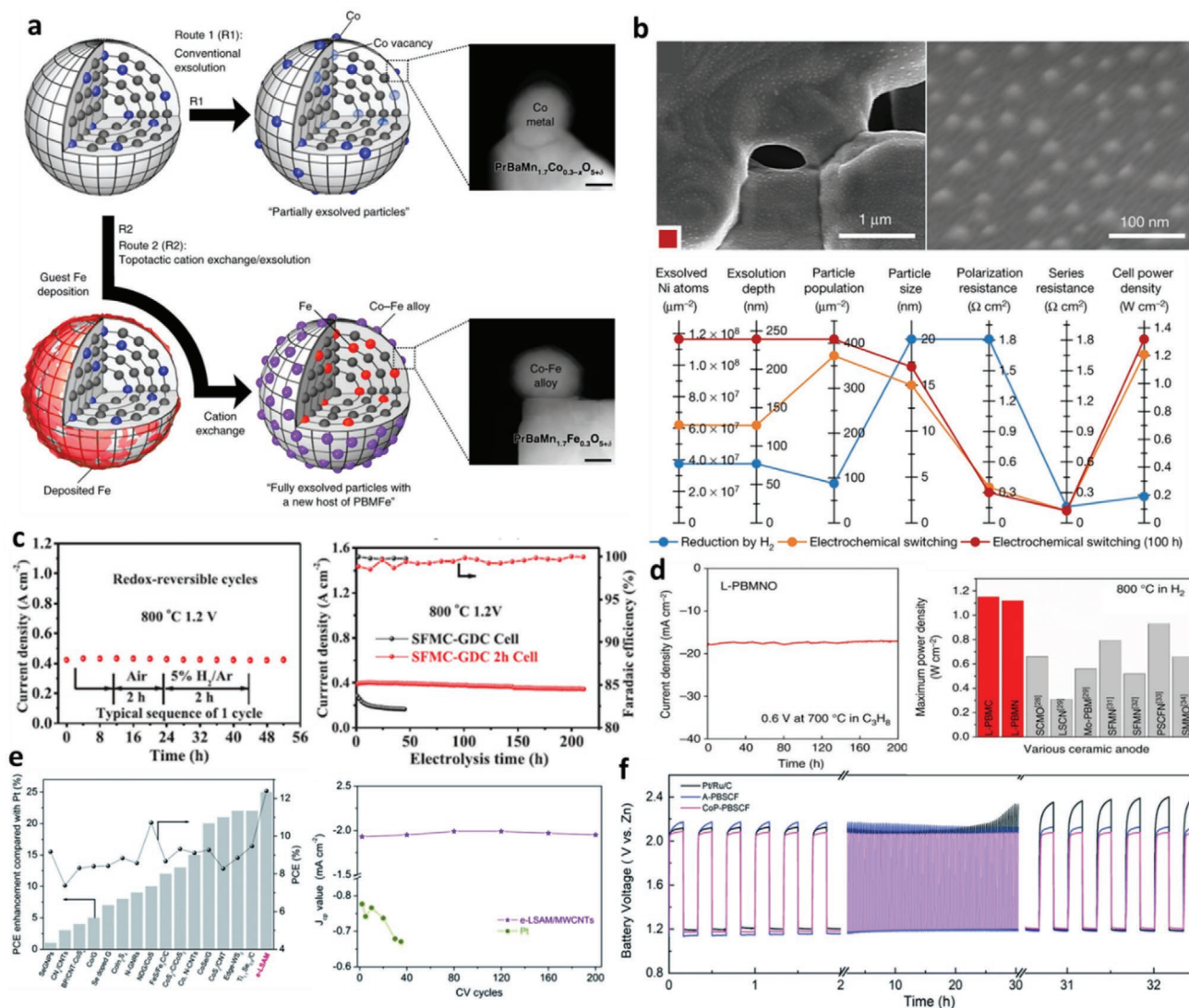


Figure 14. Exsolution in electrochemical applications. a) Schematic of the exsolution process with and without topotactic ion exchange. Adapted with permission.^[125] Copyright 2019, Springer Nature. b) Electrochemical switching; SEM micrograph of a Ni electrode produced by electrochemical switching and a parallel coordinate plot showing materials' characteristics such as exsolved Ni atoms, particle size, and population as well as their performance in SOFCs. Adapted with permission.^[16] Copyright 2016, Springer Nature. c) Stability of Co-Fe reversibly exsolved particles in CO₂ electrolysis cells; comparison of as-prepared and exsolved cells and redox cycling performance of the exsolved material. Adapted with permission.^[111] Copyright 2020, Wiley-VCH. d) Electrochemical performances of a Ni exsolved (L-PBMNO) anode in C₃H₈ and comparison of the maximum power density of this with other studies in the literature. Adapted with permission.^[61] Copyright 2017, Springer Nature. e) Ag exsolution for dye-sensitized solar cells; comparison of the performance of a Ag exsolved (La_{0.8}Sr_{0.2})_{0.95}MnO_{3-δ} cathode with typical active Pt-free cathodes and its stability as compared to Pt cathodes. Adapted with permission.^[151] Copyright 2019, Royal Society of Chemistry. f) Electrochemical performance (galvanostatic charge-discharge curves) of exsolved CoP particles in rechargeable Zn-air batteries as compared to as-prepared samples (A-PBSCF) and Pt/Ru/C air electrodes. Adapted with permission.^[122] Copyright 2019, Royal Society of Chemistry.

The SOFC cathodes have also been an area of interest although less developed than work on anodes, probably due to that fact that exsolution naturally requires reducing environments to occur. However, there have been attempts to use these materials in symmetrical SOFCs. Reports indicate improvement of the total power density as compared to conventional materials.^[86] Specifically, Ruddlesden-Popper type lanthanum strontium manganite (La_{0.5}Sr_{1.5}MnO_{4+δ}) with exsolved Ni particles exhibit improved activity for the hydrogen electro-oxidation reaction of >40% and electrocatalytic activity for oxygen

reduction reaction (ORR) of >20% due to decreased interfacial polarization resistance.^[86] However, in situ exsolution from a (La,Sr)(Ti,Ni)O_{3-δ} seems to be limited by slow kinetics and higher temperature reduction is proposed in order to make Ti⁴⁺ reduction thermodynamically possible.^[87]

Ni exsolved materials have also extensively been applied for electrolysis in solid oxide cells. The metallic Ni nanoparticles has also been shown to significantly enhance the electrode performance and elevate the current efficiency of that electrode in high-temperature steam electrolysis cells.^[54,88,89] The

presence of those electrocatalytically active, exsolved metallic Ni nanoparticles in combination with higher concentrations of oxygen vacancies seem to dramatically lower the activation barrier to steam electrolysis compared to the parent materials.^[90] For example, Ni nanoparticles exsolved from a $\text{La}_{0.4}\text{Sr}_{0.4}\text{Ti}_{0.9}\text{O}_{3-\delta}$ created a so called hybrid material where support and particles synergistically exhibit higher hydrogen evolution reaction (HER) catalytic activity and a faster charge transfer rate than the corresponding physical mixtures.^[91] CO_2 electrolysis cells have been demonstrated to display increased performance when Ni exsolved materials are used as cathodes.^[92] The n-type electrical properties of exsolved ilmenite cathode materials ($\text{Ni}_{0.9}\text{TiO}_3$) are considered responsible for increased electrochemical performance and metal nanoparticles anchored on the surface are believed to shorten the diffusion length for free electrons, all together improving the performance of the electrodes.^[93] Additionally, promotion of CO_2 adsorption/activation by making use of redox active dopants such as Mn on the B-site of a perovskite also links to enhanced electrochemical performance of the cell.^[78] Coelectrolysis of H_2O and CO_2 cells have also been demonstrated to employ exsolved Ni nanoparticles for efficient syngas generation exhibiting up to 20% improved electrocatalytic syngas production rates when compared to the commonly used Ni-YSZ while stable operation was achieved without the need for protective H_2 atmosphere.^[94]

Ni exsolution is also widely used in catalytic applications such as the transformation of hydrocarbons into valuable products especially in areas such as methane reformation or production.^[95–99] This is not surprising since Ni-containing catalysts are often considered to be state of the art for the reformation of a range of hydrocarbons (**Figure 15b**).^[100] Exsolved nickel catalysts have been employed for the conversion of some higher hydrocarbons such as ethanol^[101] and ethane.^[102] In such work, by carefully selecting the ratio between the A-site elements, control over the degree of separation/incorporation of the B-site was achieved.^[101] Additionally, when applied to the simultaneous production of ethylene and H_2 via ethane dehydrogenation, exsolved Ni particles were found to enhance both carbon resistance and dehydrogenation. Interestingly, increasing exsolved Ni surface area resulted in increased C_2H_6 conversion but decreased $\text{C}_2\text{H}_4/\text{H}_2$ selectivity, which implies that the activity is probably dictated by a balance between the state of the ions in the bulk (i.e., Ni^{2+} , Mn^{4+}), the amount of Ni exsolved and the presence of oxygen vacancies.^[102]

Despite the fact that complex perovskite structures are usually employed as parent materials to exsolve from, exsolved Ni particles have also been demonstrated to emerge from simple oxides such as CeO_2 ,^[99] MgO ,^[97] or MnO_2 ^[98] in catalytic applications despite not being able to accommodate a variety of cations in their lattices. Ni released on the surface of such oxides can exhibit high activity and stability as well as coke free operation. However, it has been shown that the controllable growth of Ni nanoparticles depends on the homogeneity of the solid solution before reduction, which by default would be better in perovskite systems. This is a result of the cation and electron transport properties that perovskites exhibit, which result in the increased homogeneity of the parent material (Section 3.1). The importance of homogeneity has been shown by sintering

the parent solid solution powder at a high temperatures (**Figure 13a**).^[97]

There are not many studies on CL that use Ni but this is an area slowly receiving increasingly more interest probably because of the possibility to design new materials. Studies here focus on the reformation of methane using air as the oxidant. Interestingly, the two studies reported in the literature that use exsolution for CL take advantage of two different aspects of exsolution. The first one uses exsolved Ni particles as active sites and oxygen reservoirs, both being essential in CL processes. An increase in the reduction temperature resulted in a decrease in particle population and an increase in particle size. This was found to have a determining effect on the selectivity and the stability of the particles.^[33] The second approach introduces a new concept, whereby metallic particles are deliberately exsolved in the bulk of the oxide matrix in addition to the surface particles. The bulk particles are used to strain the perovskite and increase the overall capacity, exchange, and stability of the system while both kinds of particle are used in combination to convert methane at unusually high, for the temperature, selectivity to syngas and stability (**Figure 6**).^[15]

The concept of exsolution has also been used in solid ion-conducting oxygen transport membranes (OTMs) to enhance catalytic activity for CH_4 partial oxidation and reforming, although currently this is not an area extensively explored. Nickel doping on the B-site of a $(\text{La},\text{Sr})(\text{Cr},\text{M},\text{Ni})\text{O}_3$ ($\text{M} = \text{Mn}, \text{Fe}$) perovskite improves the reducibility of the perovskite and results in exsolution of Ni nanoparticles.^[103] Additionally, exsolution of Ni was also used in order to promote coproduction of CO and syngas on both sides of a ceramic membrane reactor when CO_2 and CH_4 were used as fuels, respectively. Ni particles exsolved in situ under CH_4 during membrane operation were proven to enhance reaction rates and oxygen flux while being stable under hydrocarbon-containing atmospheres (**Figure 16**).^[104]

6.2. Iron

Studies using Fe exsolved particles are almost exclusively dominated by electrochemical applications.^[105–108] Fe exsolution has been demonstrated to result in some very interesting morphologies. This could be due to the ΔG value of the reduction of its corresponding oxides to metal, which is close to 0 under typical temperature and $p\text{O}_2$ for exsolution (Section 3.2). This usually results in particles comprising of mixed metallic and oxide phases. In comparison Ni has a very negative ΔG for reduction of its oxide and will always result in metallic particles. This balance of metallic and oxide phases is known to result in more faceted morphologies for such particles. For example, Fe whiskers have been exsolved from a traditional LSF material accompanied by SrO nanorods of several tenths of nanometers in length and up to 20 nm in thickness. According to a model of Fe whisker growth, the rate limiting step of the exsolution of Fe is the extraction of lattice oxygen. This favors the formation of single iron metal atoms, which in turn grow into isolated rods (**Figure 13c**).^[44] Additionally, raspberry-like exsolved iron oxide nanoparticles enable the preparation of high-surface area materials, which

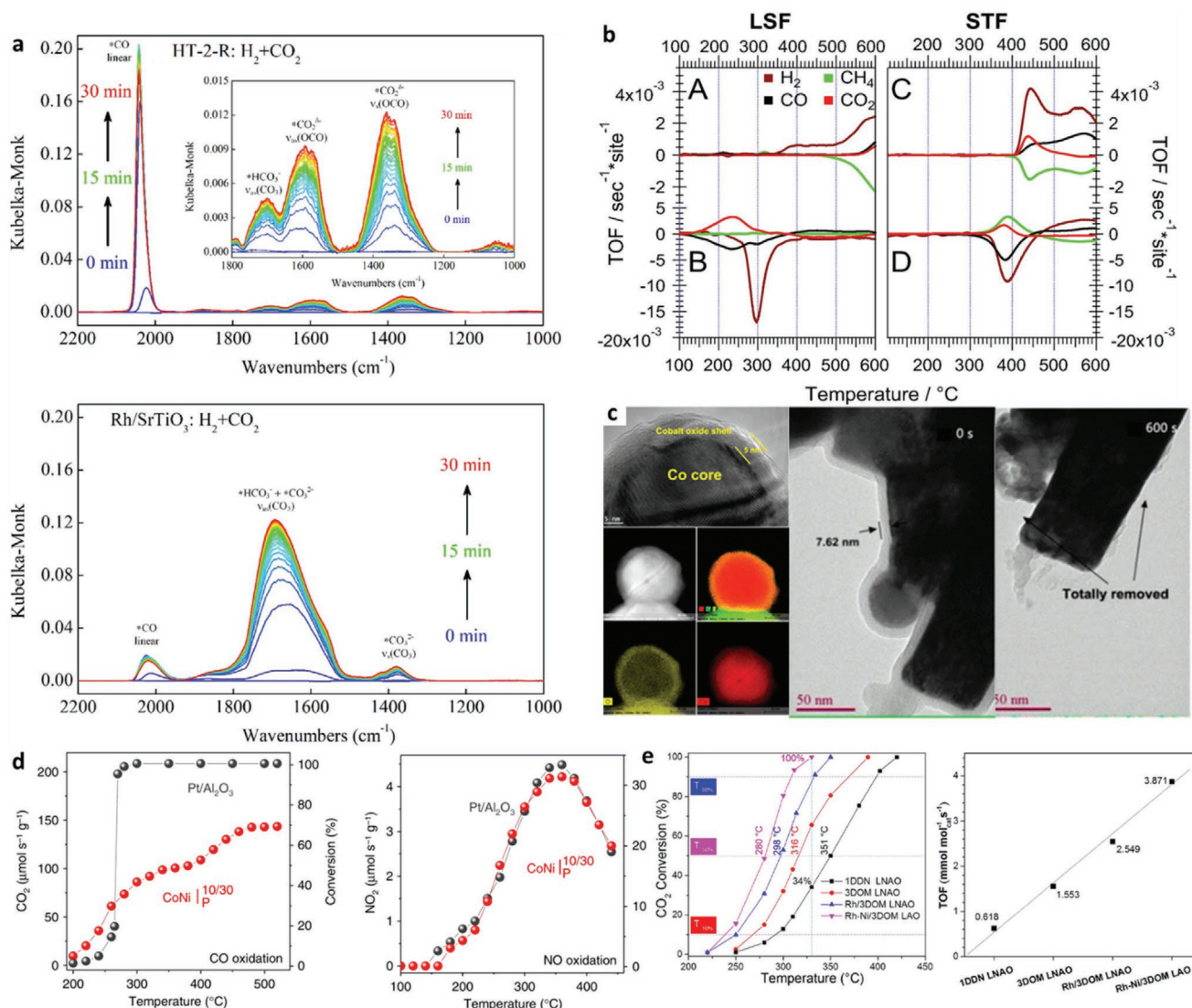


Figure 15. Exsolution in catalytic applications. a) Rh exsolution on CO₂ hydrogenation; in situ DRIFT spectra of CO₂ hydrogenation after exsolution (HT-2R exsolved sample; Rh/SrTiO₃ benchmark sample). Adapted with permission.^[66] Copyright 2018, Elsevier. b) Ni exsolution for methane steam reforming and CO methanation; reaction rates on Ni-LSF (on the left) and Ni-STF (on the right). Adapted with permission.^[100] Copyright 2016, Elsevier. c) Co exsolution for soot oxidation; high-resolution TEM images of the core-shell structure of a Co exsolved particle, high-angle annular dark field image overlaid with EDX map images, soot oxidation over time. Adapted with permission.^[123] Copyright 2016, American Chemical Society. d) Bimetallic Co-Ni exsolution for CO and NO oxidation; catalytic rates as a function of temperature.^[26] Copyright 2017, Springer Nature. e) Bimetallic Rh-Ni nanoalloys for CO₂ methanation; catalytic activities and TOF values at 330 °C. Adapted with permission.^[27] Copyright 2018, American Chemical Society.

are known to enhance the activity of ORR electrocatalysts.^[109] Specifically, they have been used to enhance the performance of N-doped carbon electrodes.^[109,110] These iron species seem to emerge from inside N-doped carbon nanoshells onto the external carbon surface, where they form stable small FeO_x nanoparticles (Figure 13d). The location (endo- or exohedral, i.e., inside or outside the carbon nanoshell, respectively) of these small, structurally stable particles is responsible for a switch of the product selectivity (from H₂O₂ to H₂O) during testing. Fe exsolution from spinel oxides has also been studied because of the relatively high electrical conductivity of spinels combined with excellent thermal and structural stability. This makes them ideal candidates for use as protective layers

on ferric stainless steel interconnects in various cathodes/cathode systems (Figure 14c).^[111] In this case, iron exsolution has been demonstrated on the surface of a spinel-type electronic conductor FeV₂O₄ by in situ reversibly reducing FeV₂O₄ to Fe + FeV₂O₄ in a reducing atmosphere.^[112]

In order to investigate Fe exsolution on different electrodes in situ X-ray photoelectron spectroscopy (XPS) has been employed.^[113,114] XPS was used to study the effect of the oxygen partial pressure on exsolution under conditions that would simulate the standard operating conditions of typical SOFC anodes or solid-oxide electrolysis cell (SOEC) cathodes. When the oxygen partial pressure on the working electrode was below the FeO/Fe redox pair, the exsolution of metallic Fe nanoparticles

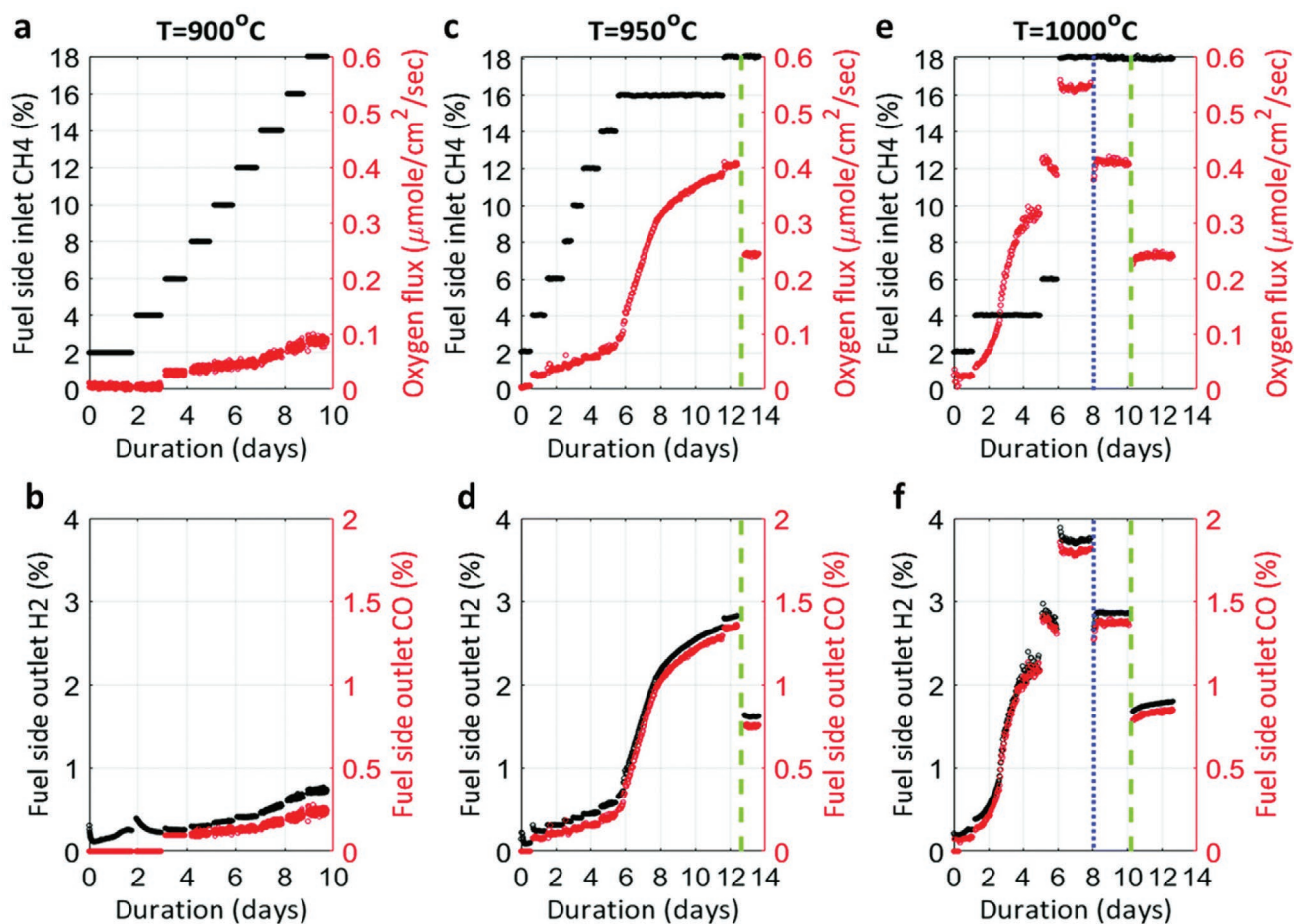


Figure 16. Exsolution in membrane applications performance of a $\text{La}_{0.85}\text{Ca}_{0.10}\text{Fe}_{0.95}\text{Ni}_{0.05}\text{O}_{3-d}$ perovskite as a function of inlet CH_4 mole fraction and time. a,c,e) Inlet CH_4 mole fraction (black) and oxygen permeation flux (red). b,d,f) H_2 (black) and CO (red) mole fractions at the outlet of the fuel side. The blue and green vertical dotted lines denote the points where the temperature is reduced from 1000 to 950 °C and from 950 to 900 °C, respectively. Reproduced with permission.^[104] Copyright 2019, Royal Society of Chemistry.

was observed.^[114] Moreover, near-ambient-pressure X-ray photoelectron spectroscopy (NAP-XPS) was used on electrochemically polarized $\text{La}_{0.6}\text{Sr}_{0.4}\text{FeO}_{3-\delta}$ (LSF) thin film electrodes that exhibited relatively high activity toward electrochemical water splitting as compared to a conventionally used, unexsolved LSF. It was demonstrated that although iron species could be reduced to metallic state, while still retaining their crystallographic positions, it is more likely to form metallic iron particles on the surface due to the tendency of Fe metal atoms to agglomerate under the investigated conditions. These metallic particles were shown to be responsible for promoting water splitting kinetics. Additionally, the Fe-depleted oxide surface after exsolution may additionally contribute, e.g., by a change in the $\text{Fe}^{+2}/\text{Fe}^{+3}$ ratio at the oxide surface upon Fe^0 formation.^[113]

6.3. Cobalt

The exsolution of Co is one of the most popular areas of research in the exsolution field and literature is quite diverse with many publications in areas of application, including, but not limited to, CO^[26,115] or soot oxidation,^[116] Zn–air batteries,^[70]

chemical looping,^[117] and fuel cells.^[118] Co particles can be active for both anode^[119] and the cathode^[120] as well as in symmetrical cells^[121] in SOFCs.

When used in Zn–air batteries, materials with exsolved cobalt particles are reported to deliver high power density and remarkable mechanical flexibility under different conditions.^[70] One very interesting study transforms the exsolved Co particles into CoP particles with an intriguing “postgrowth” approach in order to use them in such batteries. This is essentially a similar approach to the “chemistry at a point” concept^[26] (Section 2.2) where the authors take advantage of the strong anchorage of the exsolved particles and subject them to further treatments, in this case phosphatization. CoP and oxygen vacancies modify the electronic configuration of the catalysts and the reactants adsorbed on their surface. An increased amount of adsorbed H_2O and oxygen/hydroxyl was found on the surface of the reduced and phosphorized materials, suggesting a strong hydrophilic nature, which with the surface oxygen vacancies play an important role in enhancing catalytic activity. The intimate interpenetration of these two components, resulting from the strong interaction of the exsolved particles and the support (Section 2.2), yields synergistically active

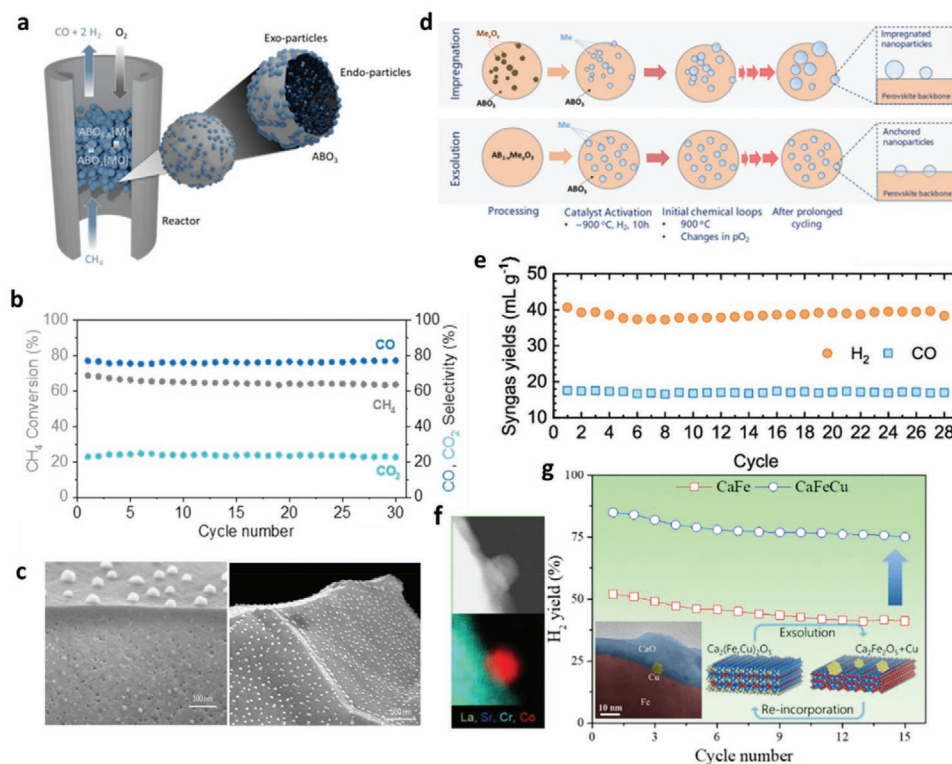


Figure 17. Exsolution in chemical looping applications. a) Schematic representation of chemical looping via exsolved endo/exoparticle systems. b) Stability in methane partial oxidation to syngas via chemical looping, conversion of CH_4 , and selectivity to CO and CO_2 with cycle number. c) SEM micrograph cross-section view after exsolution revealing surface and bulk particles. Adapted with permission.^[28] Copyright 2020, Royal Society of Chemistry. d) Schematic comparing the main differences between exsolution and impregnation cermet manufacturing on the catalytic nanoparticle stability in a chemical looping operation. e) CO , H_2 production during the methane partial oxidation half cycle of a 28-cycle chemical looping methane reforming test. f) HAADF-STEM image and EDS mapping after exsolution. Adapted with permission.^[117] Copyright 2020, American Chemical Society. g) A reversible calcium–iron-based oxygen carrier with exsolved Cu nanoparticles used for methane oxidation. Adapted with permission.^[129] Copyright 2020, American Chemical Society.

sites, which results in excellent performance toward the oxygen reduction/evolution reaction (ORR/OER) and HER. The CoP – $PrBa_{0.5}Sr_{0.5}Co_{1.5}Fe_{0.5}O_{5+\delta}$ electrode prepared here demonstrates a high power density, a competitive charge/discharge polarization, and a superior stability compared to commercial $Pt/Ru/C$ in Zn –air batteries. Moreover, it shows a low overpotential in overall water splitting, surpassing most reported electrocatalysts. The homogeneous incorporation of metallic CoP is also expected to provide an optimized electron transfer path and an improved conductivity (Figure 14f).^[122]

For catalytic applications exsolved systems have been used in soot and CO oxidation and Fischer–Tropsch reactions where the $LaFe_{1-x}Co_xO_3$ perovskites yielded a wide distribution of liquid hydrocarbons (C_6 – C_{18+}) and high CH_4 formation (Figures 13b and 15c,d).^[26,116,123] Decreasing the particle size of Co favors the formation of longer chain hydrocarbons at the expense of the CH_4 selectivity providing a way to control selectivity through particle size.^[124] In another study where Co exsolved particles proved to have relatively high activity for CO oxidation, XPS and X-ray absorption near-edge structure analysis (XANES) were employed in order to confirm that the enhanced activity was a result of a synergetic effect between the surface oxygen of $LaCoO_3/Co_3O_4$ and Co^{3+} in the Co_3O_4 nanoparticles.^[115] The combined effect of the oxygen vacancies and the surface cobalt

oxide layer on the catalytic activity of such systems was also demonstrated in soot combustion^[123] where the exsolution of Co species facilitated further mobility of the adsorbed oxygen species through spillover phenomena thus increasing the activity of the whole surface.

Both concepts of irreversible and reversible exsolution have been used with Co containing materials for chemical looping applications. In the former case, Ni – Co alloyed particles exsolved from a titanate lattice and by employing the endo/exoparticle method the material achieves highly selective methane conversion at $450^\circ C$.^[28] In the latter case, exsolved Co nanoparticles on a chromate matrix exhibit microstructural stability and a twofold improvement over the bare perovskite in activity for redox dry methane conversion (Figure 17a–f).^[117]

Last, topotactic exsolution was employed in order to prepare systems with exsolved cobalt, and the materials exhibited increased electrochemical activity and catalytic activity toward the reformation of methane when compared to other recently developed ceramic anodes. It was demonstrated that due to favorable incorporation energy, Co species in $PrBaMn_{1.7}Co_{0.3}O_{5+\delta}$ can be exchanged with surface deposited Fe species (Figure 14a), leading to a $PrBaMn_{1.7}Fe_{0.3}O_{5+\delta}$ matrix, with exsolved Co particles.^[125]

6.4. Copper

Copper forms one of the most reducible first transition metal row oxides (Section 3.2; Figure 7b), which should make it an ideal candidate for exsolution. Indeed, exsolution of copper has been one of the first non-noble metals studied (2012) but the idea has not been developed to any extent since. This is probably because Cu is also notoriously mobile, leading to agglomeration and stabilizing it, even by exsolution, has been a challenge in catalysis and electrochemistry for quite some time. However, in an attempt to make controllable copper exsolution possible, various matrixes have been employed including chromates,^[74,126] titanates,^[13,127] or ferrites.^[128] Cu exsolution studies remain very limited in number, accounting for only about 5% of the non-noble metal-based studies published.

One way to alleviate agglomeration issues inherent to Cu is to employ the reversible exsolution concept discussed in Section 2.2. This was exemplified for chemical looping methane conversion, where Cu exsolved $\text{Ca}_2\text{Fe}_2\text{O}_5$ demonstrated a high and cyclically stable yield of H_2 , as the exsolution of Cu particles is thought to increase the reducibility of $\text{Ca}_2\text{Fe}_2\text{O}_5$ under CH_4 (Figure 17g). The stable redox performance of the oxygen carriers is attributed to the reversible exsolution and reincorporation of Cu nanoparticles however oxidizing the reduced materials with CO_2 only is not sufficient to reincorporate the Cu nanoparticles and an additional air oxidation step is required.^[129]

Cu exsolution has also been used for electrochemical applications, where the main advantages highlighted in literature included coke and sulfur resistant^[128] performance in reversible, intermediate temperature SOFCs, agglomeration resistant properties in high temperature steam electrolysis^[13,127] and increased conductivity and stability in ceramic fuel electrodes.^[13] This was mainly attributed to the synergetic effect of the metallic catalyst and the ceramic support as well as a shortening in the diffusion length of free electrons in the ceramic, which has been shown to favor the conductivity increase of the samples.^[127]

6.5. Other Elements or Compounds

Without a doubt the overwhelming majority of published research on the area focuses on the exsolution of Ni, Co and Fe. However, there are also some reports of other metals compounds or metal oxides being exsolved, which will be mentioned in this section, with most of them focusing mainly in electrochemical applications.

For example, a cubic $\text{Nd}_{0.5}\text{Ba}_{0.5}\text{MnO}_3$ was prepared aiming to exsolve Mn-based particles for a SOFC anode. It was shown that the perovskite undergoes a phase transition when the nanoparticles are released and forms a layered perovskite structure. The newly formed MnO nanoparticle-decorated perovskite was employed in the anode and exhibited excellent power generation performance even without any additional oxidation catalysts.^[130] Reversible Mo exsolution was also observed under SOFC operation, which majorly enhanced the electrochemical activity of $\text{Sr}_{1-x}\text{Ca}_x\text{MoO}_3$ toward H_2 and CH_4 oxidation.^[131] As mentioned in Section 3.1, perovskite oxides are able to accommodate a wide range of A- and O-site nonstoichiometries that allow bulk transport

of B-site cations and surface nucleation, hence different exsolution pathways may be possible. For example, SrO nanoislands exsolved from A-site excess perovskites display enhanced activity toward CO_2 reduction due to the fact that they enable high-temperature chemical CO_2 adsorption and activation.^[132] Additionally, formation of SrO rods following reduction in dry hydrogen seems to be enabled by the presence of surface Ni particles. The mechanistic aspect of rod growth is thought to mimic a surface diffusion-controlled carbon whisker growth on Ni, leading to similar extrusion rods and filaments (Figure 13c).^[44] PrO_x particles exsolved from a $\text{PrNi}_{0.5}\text{Mn}_{0.5}\text{O}_3$ (PNM) matrix dramatically enhance both the ORR kinetics and stability of the state-of-the-art LSCF cathode by working synergistically with the support. The particles incorporate a high concentration of oxygen vacancies while the thin PNM film effectively suppresses Sr segregation from the LSCF phase, thus significantly enhancing the stability of the cathode.^[133] Last, preparation of WS_2 nanodots was employed in the design of a photocatalytic system. In particular, the authors treat a W-modified SrTiO_3 with CS_2 combining at the same time in situ exsolution and sulfurization hence employing the “chemistry at a point concept” (Section 2.2) to create new nanostructures that preserve their initial locations. The socketed nature of the nanodots provides abundant coupling interfaces in the heterostructure, which promote the visible light absorption and photocatalytic performance. It is also suggested that the presence of WS_2 nanodots suppresses the recombination of photogenerated charge carriers, which leads to a larger amount of mobile electrons, hence increasing the efficiency of the photocatalyst (Figure 18a–c).^[65]

7. Noble Metal Systems and Their Applications

As opposed to non-noble metals, due to their much more negative ΔG of their oxide reduction (Figure 7b), noble metals are much more prone to exsolve in the bulk rather than on the surface, which means that their exsolution is not really reversible but rather, a high amount of the substituted metal ends up being trapped as metal particles in the bulk of the support matrixes,^[25] which could make them inaccessible for many catalytic applications. Additionally, a possible explanation for the poor reversibility of these systems is the fact that the ionic radii of the noble metal (Figure 9a) is slightly larger when compared to metals that are usually substituted on the B-site of a perovskite (Section 3.2). Generally, most of the matrixes that are employed as backbone structures are redox active like Fe and Mn in order to allow reversible exsolution. Ti-based materials are also commonly used in order to serve mostly as support and provide more stability, although not redox active. Looking at the applications of noble metal exsolution, electrochemistry and catalysis share the majority of the published literature. Membranes and CL are missing here mainly because they pose additional requirements such as oxygen capacity and it would not be cost efficient to use a noble metal only for that oxygen capacity. Generally, Pd is the most common noble metal used; reports on Rh, Ru, Ag, and Pt are quite similar in numbers while there are only two published studies for Ir exsolution.

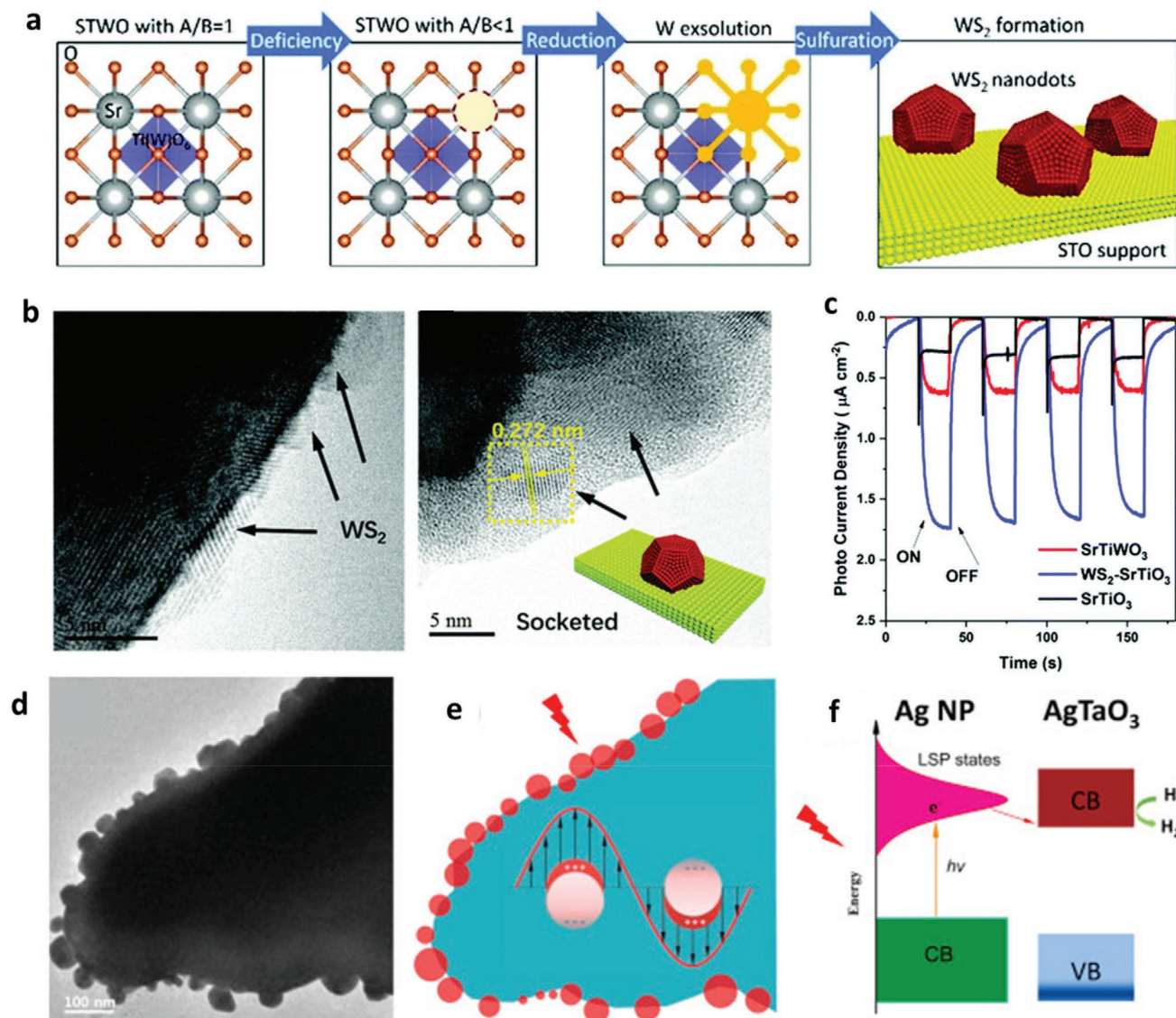


Figure 18. Exsolution in photocatalytic applications. a) Schematic illustration of the new formation strategy of a WS_2 -anchored- SrTiO_3 heterostructure via in situ exsolution. b) High-resolution TEM (HR-TEM) images of in situ grown WS_2 nanodots anchored on WS_2 - SrTiO_3 sample image of WS_2 . c) Photocurrent tests showing WS_2 - SrTiO_3 displays an enhanced separation efficiency. Adapted with permission.^[65] Copyright 2018, Royal Society of Chemistry. d) TEM image of a bulk AgTaO_3 particle with silver nanoparticle grown on the surface. e) Image of silver nanoparticles excited by electromagnetic field of visible light photons. f) Representation of direct injection of excited free electrons in the silver into conduction band of AgTaO_3 . Adapted with permission.^[149] Copyright 2015, Elsevier.

7.1. Palladium

Pd is mainly used in catalytic applications including CO oxidation, methane conversion, and de- NO_x processes although there are also some studies where it is used for SOFCs or sensors. Notably, Pd is usually substituted in stoichiometric compositions attempting to take advantage of the reversible exsolution concept (Section 2.2).

The state of palladium has been followed under operando conditions using X-ray absorption near edge structure (XANES) and quick scanning extended X-ray absorption fine structure (QEXAFS) at the Pd K-edge combined with mass spectrometry (MS) in a methane conversion process. Exsolved Pd reversibly

emerges from a LaFeO_3 surface under reducing conditions and enters the LaFeO_3 structure under oxidizing conditions while infiltrated Pd oscillates between the reduced and partially oxidized state. This structural difference is thought to be responsible for an activity enhancement and is attributed to the self-regenerative property of perovskite-type oxides.^[134] These self-generative properties seem to also be responsible for excellent NO_x reduction activity for lean-burn exhausts with NO_x conversion and N_2 selectivity >90% over a wide operating temperature range, as well as an extremely high sulfur tolerance properties.^[135] Additionally, some of the very first publications on exsolution were on CO oxidation, which is also known to be sensitive to the state of the active metal. In this case, it was demonstrated that Pd doping

significantly promotes the mobility of oxygen species in the perovskites^[57,136] while partially reduced Pd species or extremely small particles (<1 nm) strongly interacting with the surface were thought to be responsible for the low temperature activity.^[136]

Similar enhanced activity was demonstrated for Pd exsolved systems for electrochemical applications. In sensors, the decoration of PdO nanoparticles enhanced the response signal accompanied by improved sensitivity and detection limit due to the improved electrocatalytic activity of the materials.^[137] The formation of Pd nanoparticles, which self-recovered through reoxidation and reduction cycles, were found to be responsible for long-term stability and recovered power density upon exposure of the anode to air.^[138,139]

7.2. Rhodium

Despite the fact that Rh can be easier accommodated at the perovskite B-site as compared to Pd^[140] due to size and coordination number (Figure 7a) it has not been studied to the same extent as other noble metals. Interestingly, the majority of the studies published on Rh exsolution are mainly on catalytic conversion processes such as CH₄ steam reforming^[141] and CO₂ reduction^[66] either as a single metal or as a bimetallic catalyst^[27,66] (Figure 15a,e). In CH₄ steam reforming increased activity seems to originate from the use of the reversible exsolution concept^[141] while in CO₂ reduction the key to increased activity are subnanometer Rh clusters, which are produced by concept controlled reduction of Rh-doped perovskites using the irreversible exsolution concept.^[142] In particular, in the latter case, more sites for the activation of H₂ (and C₂H₆) are created while at the same time the crystallographic alignment between Rh atoms and support assist in regulating the binding energies of adsorbates.^[66]

Additionally, as with all noble metal applications, their efficient use will always be a key focus of material design. Exsolution from dilute compositions poses additional requirements due to the nature of the process and the strong interactions between the dilute exsolvable ion and the host matrix. These kinds of interaction and opportunities have been studied for CO oxidation processes. Exsolved materials were able to compete well against conventionally prepared samples with much higher apparent surface loading of noble metal.^[42] This suggests that it is not only the amount of noble metal sites that are accessible to reactants for activity but also the state of the noble metal and the nature of the active sites, which is possibly affected by the strain that noble metal particles experience.

Last, there is one example of exsolution of Rh for electrochemistry, which employed the concept of symmetrical exsolution in SOFCs for syngas production from greenhouse gases, which enabled syngas and electricity cogeneration.^[43]

7.3. Ruthenium

Ruthenium exsolution has been mainly employed for electrochemical applications and a few studies on methane reformation.

The range of electrochemical applications where exsolution of Ru is used is vast ranging from NH₃ synthesis,^[143] to direct ethanol fuel cells^[144] or OER cells.^[145] In all cases increase of the

electrochemical activity is reported as a result of the enhancement of the electronic conductivity of the materials upon Ru doping.^[144,145] This is believed to occur due to the distortion of the BO₆ octahedron inflicted by the substitution of B-site ions (i.e., Mn) with Ru.^[146] In addition the release of Ru nanoparticles on the surface of the perovskite oxides enhances the electrocatalytic activity of the materials because these newly formed particles correspond to additional active sites.^[143–145]

Use of exsolved Ru nanoparticle systems in methane conversion processes demonstrate high conversions, yields and remarkable stability. Ru nanoparticles exsolved from Sr_{0.92}Y_{0.08}Ti_{1-x}Ru_xO_{3-d}^[147] or Sm₂Ru_xCe_{2-x}O₇^[148] perovskites exhibited superior performance, which was accredited to their high resistance to sintering-induced deactivation as a result of the stabilizing metal–support interaction in this class of materials.

7.4. Silver

As compared to all other noble metals silver is mainly substituted on the A-site of a perovskite structure due to its larger ionic size (Section 3.2; Figure 7a). However, preparation and consequent exsolution of Ag-based materials is difficult to control since AgO spontaneously converts to Ag at about 400 °C. Ag exsolution is mainly used in photocatalytic applications and sensors with a few studies on the ORR. Exsolved silver nanoparticles have been shown to induce photocatalytic activity. In particular, in photocatalytic water splitting exsolved silver nanoparticles are reported to strengthen the visible light absorption due to localized surface plasmons of the nanoparticles (Figure 18d–f).^[149] This is thought to improve activity toward both photocatalytic hydrogen and oxygen production under visible light illumination ($\lambda \geq 400$ nm).^[150] Furthermore, when applied for the electrocatalytic triiodide reduction for dye-sensitized solar cells, they achieve 25% enhancement in activity as compared to any Pt-free cathodes as well as superior durability to that of the Pt electrode, which is considered to be the state of the art (Figure 14e).^[151]

Similar to the Ru materials discussed above, when applied for ORR, exsolved Ag nanoparticles are reported to be “extraordinarily” stable and serve as both active reaction sites and prime electron-transfer pathways while providing strong anchoring, effectively mitigating the known instability of Ag.^[69,71,152,153] Last, decoration of NH₃ sensor electrodes with Ag nanoparticles has been reported to enhance the response signal (electric potential difference) of the sensor accompanied by improved sensitivity, and detection limit as well as outstanding selectivity to NH₃ against NO₂. The anti-interference capability of the sensor toward NO and NO₂ is effectively enhanced due to the improved adsorption and electrocatalytic activity of the materials.^[154]

7.5. Iridium

To the best of our knowledge, there are only three papers published on Ir exsolution, which focus on catalytic applications, one on the ability of this noble metal catalyst to efficiently

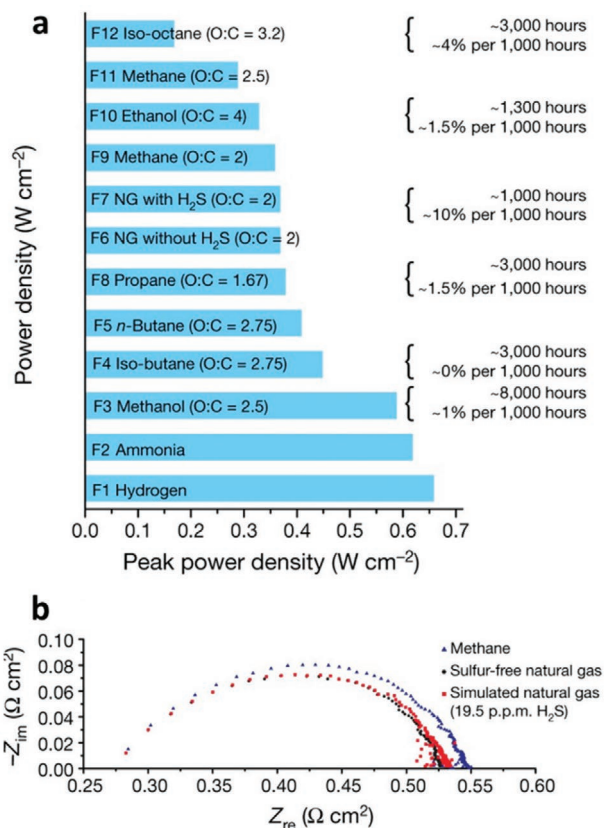


Figure 19. Durability of exsolved materials. PCFC performance across a range of fuels. a) Peak power densities of PCFCs on 12 different fuel streams at 600 °C (methane is shown for two different O:C ratios). Life-time and degradation rate of PCFCs on selected fuels also indicated. NG, natural gas. b) Nyquist plots of a PCFC under sulfur-free simulated natural gas, simulated natural gas with H₂S, and methane. Z_{im} is the imaginary component and Z_{re} is the real component of impedance. Adapted with permission.^[79] Copyright 2018, Springer Nature.

convert CH₄ using CO₂^[155] and the other two on CO oxidation.^[156,157] In all cases, it is demonstrated that the improved catalytic activity of the material was induced after the emergence of the Ir nanoparticles on the surface. In the former case this was shown to be due to the particles' ability to catalyze the cleavage of the C–H bond in CH₄ with high coking resistance. In the latter, the high activity displayed by the system was explained by the strained nature of the exsolved nanoparticles when compared to ones prepared by deposition.

8. Durability of Exsolved Materials

Initially, the stability of exsolved materials was discussed in relation to their reversibility, i.e., particles being able to redissolve in the lattice under oxidizing condition rather than coarsen. Later, when the concept of irreversible exsolution was introduced, stability was a result of the socketed nature of the exsolved particles that protected them from agglomeration and carbon deposition (discussed in Section 2.2). For these reasons, they have been reported to be extremely stable in a vast number of applications ranging from electrochemistry to hydrocarbon catalysis

and redox cycling applications as compared to their impregnated counterparts, as evidenced by the fact that about 30% of the papers on exsolution include some form of stability study. A study published in 2015 revealed for the first time that the stability observed in exsolved particles was a result of the socketing and alignment of those particles with the parent perovskite.^[11]

Catalysts (especially Ni-based) used in reactions such as hydrocarbon reforming and CO oxidation can suffer from deactivation due to catalyst sintering, carbon deposition, and sulfur poisoning. However, the catalysts prepared via exsolution are reported to exhibit enhanced durability due to the fact that their alignment with the support can alter the carbon deposition mechanism^[11] and also prevent agglomeration. For example, in hydrocarbon environments Ni supported catalysts are reported to maintain almost full conversion of CH₄ for 1000 h at 750 °C^[97] and operation for over 360 h at 700 °C with only slight degradation (<10%) under CH₄ and CO₂ feed.^[158] Moreover, the Ni decorated La_{0.7}Ca_{0.3}Fe_{0.7}Ni_{0.3}O₃ catalyst was highly stable for oxidative steam reforming of ethanol for 200 h at 650 °C.^[101] Last, in CO oxidation the exsolved CoNi^[26] maintained CO oxidation activity for over 650 h at 220 °C. In redox conditions, a Ni exsolved system exhibits high stability in partial oxidation of CH₄ over 130 redox cycles at 570 °C.^[15]

Impressively, in a long-term stability study of PCFCs using an in situ exsolved Ni-doped BaZr_{0.8}Y_{0.2}O_{3-δ} anode the cell performance was evaluated in 11 different fuels at temperatures between 500 and 600 °C for thousands of hours (~8000 h in methanol), and demonstrated the extraordinary durability, coking resistance, and sulfur tolerance of the cells during the long-term operations (Figure 19).^[79] In SOFCs anodes, Sr₂Fe_{1.5}Mo_{0.5}O_{6-δ}-Gd_{0.1}Ce_{0.9}O_{1.95} with exsolved Fe nanoparticles, exhibited stable performance and sulfur tolerance in H₂ fuel over 700 h at 600 °C^[159] and CoFe nanoparticles were stable in different fuels (H₂, C₃H₈, and JP8) at 800 °C without any notable carbon deposition over 550, 100, and 20 h, respectively.^[32] At the same time, exsolved PrO_x nanoparticles showed high activity and stability for oxygen reduction reaction for 500 h at 750 °C when used in SOFC cathodes.^[133] In SOECs, NiFe nanoparticles exsolved from Sr_{1.9}Fe_{1.5}Mo_{0.4}Ni_{0.1}O_{6-δ} support exhibited stable cell performance for 500 h under harsh conditions in direct CO₂ electrolysis^[160] while in symmetrical cells Rh exsolved materials were coke free and stable over the 96 h operation at 850 °C.^[43]

9. Conclusions and Future Directions of Research

9.1. Overview

More than 300 studies have been published on exsolution since the first reports back in 2010, making this a fast-growing field. In spite of being so relatively new, the field is strongly application-driven aiming to take advantage of the unique functional capabilities and less focused on mechanistic insight or modeling of the process. Nevertheless, these key areas will have to be further developed in the near future. The scientific community has obviously realized the potential of these materials but unless their design and formation principles are not understood, this will prevent the development of more

advanced exsolved systems and the discovery of additional beneficial properties.

9.2. Mechanistic Understanding and Modeling

While the nucleation and growth of particles and their respective sockets have been already documented, questions still remain in terms of the exact role of temperature and time on particle size and population control. Moreover, there is a clear gap in the understanding and modeling of atomic scale processes that underpin exsolution, including cation diffusion, anion diffusion, electron delocalization, and filling of the electronic band structure states, especially in heavily defective systems. There has also been little work performed on simulating, and indeed observing, the effect of different types of driving forces, and their magnitudes, required to trigger exsolution.

Another aspect fundamental to exsolved particles is the degree of strain they are subjected to in the socket, which is rarely sufficiently quantified and linked quantitatively to catalytic reactivity. This is especially important given the recent report that shows that the degree of particle immersion and presumably the strain could therefore be controlled.^[14] There is also still much work to be done toward understanding which sites on the exsolved particles exhibit higher reactivity—while different sites will experience different degrees of strain.

Last but not least, one would ultimately also want to be able to model the resulting microstructures and nanostructures given a material prepared by a given route (with its characteristic grain, crystallite size, internal defects, and surface structure and composition) when exposed to a given set of external conditions, as outlined above.

9.3. Diversifying Exsolved Structures and Functionalities

Exsolution is clearly already a very powerful platform for creating a very diverse range of materials, however, there is scope for potentially ground-breaking new materials when considering it holistically. Through the combination of a given parent lattice with its own functionality (ionic, electronic, magnetic, thermoelectric, photoelectric, dielectric, etc., properties) and the range of external control factors, a range of nano-microstructures can be decorated with particles of different size, population, and more recently shape, on the surface but also within the bulk. This could allow the coupling of functionalities within the same structure, otherwise not possible through other means and increase the applicability of exsolved materials in various fields with specific material requirements.

The diversity of exsolved materials can be further extended by considering other crystal structures or related structures to the ones already investigated. For example, perovskites have a wide range of related structures and defect chemistries relevant for many energy conversion applications due to ion and electron transport, including the Ruddlesden–Popper and Aurivillius phases. The concept could be further extended to the related, but yet distinctive halide perovskite systems heavily employed for photocatalytic applications. Spinel and fluorite

structures deserve further attention due to the opportunities they present in terms of chemistry, easier preparation and different ion transport mechanisms, thus potentially enabling lower temperature exsolution.

9.4. Extrinsic Control Parameters

One recent development shows the possibility of choosing the shape of the exsolved nanoparticles by controlling the gas environment of exsolution. This could be one of the most interesting future directions of the field since it is known that there are many catalytic processes that are sensitive to specific facets of the active sites, inducing high activity or selectivity depending on the exposed orientation of the active site. For example, the origin of enhanced photoelectrochemical (PEC) water splitting and photocatalytic dye degradation activity is thought to be the [100] facet of NaNbO_3 in a core–shell material.^[161]

Additionally, after electrochemical switching, in which one can induce the formation of hundreds of particles per square micrometer in a matter of seconds, exploring alternative ways to provoke exsolution can be particularly exciting. For example, photoinduced exsolution was recently proposed and could be an exciting future direction, and not only in photocatalytic applications, mainly because of the low temperature requirements that could allow for a whole wealth of heat-sensitive materials to be employed. The use of plasmas to drive exsolution has also recently been reported and could be a way to steer away from the need of a reducing gas environment, further simplifying the exsolution process requirements.^[162]

9.5. Synthesis Methods

Many different methods have been employed so far in order to prepare the parent matrix that will be used for exsolution, mainly corresponding to variations of the sol–gel or solid state synthesis methods. New successful synthetic methods will have to be able to control the interplay between preserving stoichiometry and lattice defects, while maximizing surface area, which indicates that the future lies in soft chemistry synthesis routes. These kinds of synthesis methods will enable lower temperature formation of materials, which will in turn permit the use of more active elements while at the same time, higher surface area will also allow for more active materials. Additionally, as these materials move closer to applications, scaled-up synthetic methods will be needed.

9.6. Areas of Application

As discussed in the previous sections, exsolution has been used overwhelmingly in electrochemical applications. Although energy conversion is of high interest there are other kinds of processes that fall into this category but are still underrepresented such as chemical looping and photocatalysis. Although they are sectors that have potentially more stringent requirements they are also receiving increasing interest due to the advantages exsolved materials can bring with them.

In terms of applications, Ni, Co, and Fe are the most commonly exsolved elements, which is not surprising if one considers the vast range of processes they are active for, including but not limited to electrochemical conversion and hydrocarbon catalysis. Ni materials for example are state of the art for hydrocarbon reformation but studies that apply exsolution to such processes are almost exclusively limited to methane conversion. Therefore, taking into account the exceptional carbon and sulfur resistivity of these materials, an obvious step is the employment of such materials for the catalysis of higher hydrocarbons such as LPG or glycerol reforming; such work has not yet been performed. Additionally, the exsolution method could be ideal for stabilizing notoriously unstable, agglomeration-prone metals such as copper, a topic what has yet to be sufficiently developed. Considering how active copper is for crucial industrial processes such as the water gas shift reaction or CO₂ hydrogenation, future research could take advantage of the stability the socketing nature of the exsolved particles offers in order to stabilize the metal and induce the long-sought stability.

In terms of noble metal exsolution applications, the studies are almost equally split between almost all the commonly used noble metals with Pd being just at the top of the list. The exception to this is Ir which, despite the fact that is generally considered very active for electrochemical water splitting, there are no studies to the best of our knowledge that attempt to combine its known activity with the expected stability of exsolved Ir nanoparticles.

Generally, noble metals are known to be very active but suffer from deactivation due to unwanted oxidation and agglomeration. In addition, they are more rare and expensive. Exsolution could be an ideal method to make more efficient use out of noble metals since it allows for enhanced stability due to the socketing nature of the active particles. Noble metals are known to be more difficult to exsolve especially from dilute compositions due to strong interactions between the ions and the perovskite matrix but also because of their tendency to decompose and remain in the bulk of materials as well. The search for low temperature-high surface area synthesis methods are especially important for this class of metals in order to produce such nanostructures.

Last, over the last year, the use of exsolution to controllably disperse metallic nanoparticles in the bulk of the oxide matrix as well as in the surface introduced completely new design opportunities of composite materials and has unlocked ion exchange and storage properties previously unknown to these materials. Since the dispersion of strained nanoparticles on the surface of oxides is beginning to revolutionize catalytic properties, one can imagine that bulk-embedded nanoparticles could be equally transformative for bulk properties of materials. Furthermore, this approach will lead to interest in using exsolution to tailor other bulk physical properties such as magnetic properties. and The determination of such properties will naturally lead to the greater availability of advanced characterization methods for these systems.^[29,30]

Supporting Information

Supporting Information is available from the Wiley Online Library or from the author.

Acknowledgements

The research leading to these results received funding from the Engineering & Physical Sciences Research Council (EPSRC) via grants EP/P007767/1, EP/P009050/1, EP/P024807/1, and EP/R023921/1. I.S.M. acknowledges funding from the Royal Academy of Engineering through a Chair in Emerging Technologies award entitled "Engineering chemical reactor technologies for a low-carbon energy future," grant number CIET1819\2\57.

Conflict of Interest

The authors declare no conflict of interest.

Keywords

energy conversion, exsolution, nanomaterials

Received: October 18, 2020

Revised: January 29, 2021

Published online:

- [1] R. T. Hannagan, G. Giannakakis, M. Flytzani-Stephanopoulos, E. C. H. Sykes, *Chem. Rev.* **2020**, *120*, 12044.
- [2] A. Wang, J. Li, T. Zhang, *Nat. Rev. Chem.* **2018**, *2*, 65.
- [3] R. Ghosh Chaudhuri, S. Paria, *Chem. Rev.* **2012**, *112*, 2373.
- [4] X. Yang, J.-K. Sun, M. Kitta, H. Pang, Q. Xu, *Nat. Catal.* **2018**, *1*, 214.
- [5] D. Neagu, G. Tsekouras, D. N. Miller, H. Ménard, J. T. S. Irvine, *Nat. Chem.* **2013**, *5*, 916.
- [6] M. B. Katz, G. W. Graham, Y. Duan, H. Liu, C. Adamo, D. G. Schlom, X. Pan, *J. Am. Chem. Soc.* **2011**, *133*, 18090.
- [7] I. Hamada, A. Uozumi, Y. Morikawa, A. Yanase, H. Katayama-Yoshida, *J. Am. Chem. Soc.* **2011**, *133*, 18506.
- [8] R. Shiozaki, A. G. Andersen, T. Hayakawa, S. Hamakawa, K. Suzuki, M. Shimizu, K. Takehira, *J. Chem. Soc., Faraday Trans.* **1997**, *93*, 3235.
- [9] Y. Nishihata, J. Mizuki, T. Akao, H. Tanaka, M. Uenishi, M. Kimura, T. Okamoto, N. Hamada, *Nature* **2002**, *418*, 164.
- [10] B. D. Madsen, W. Kobsiriphat, Y. Wang, L. D. Marks, S. A. Barnett, *J. Power Sources* **2007**, *166*, 64.
- [11] D. Neagu, T.-S. Oh, D. N. Miller, H. Ménard, S. M. Bukhari, S. R. Gamble, R. J. Gorte, J. M. Vohs, J. T. S. Irvine, *Nat. Commun.* **2015**, *6*, 8120.
- [12] D. Burnat, R. Kontic, L. Holzer, P. Steiger, D. Ferri, A. Heel, *J. Mater. Chem. A* **2016**, *4*, 11939.
- [13] S. Li, Q. Qin, K. Xie, Y. Wang, Y. Wu, *J. Mater. Chem. A* **2013**, *1*, 8984.
- [14] H. Han, J. Park, S. Y. Nam, K. J. Kim, G. M. Choi, S. S. P. Parkin, H. M. Jang, J. T. S. Irvine, *Nat. Commun.* **2019**, *10*, 1471.
- [15] K. Kousi, D. Neagu, L. Bekris, E. I. Papaioannou, I. S. Metcalfe, *Angew. Chem., Int. Ed.* **2020**, *59*, 2510.
- [16] J. Myung, D. Neagu, D. N. Miller, J. T. S. Irvine, *Nature* **2016**, *537*, 528.
- [17] K. Kim, C. Lim, J. W. Han, *Korean J. Chem. Eng.* **2020**, *37*, 1295.
- [18] B. A. Rosen, *Electrochem* **2020**, *1*, 32.
- [19] O. Kwon, S. Joo, S. Choi, S. Sengodan, G. Kim, *J. Phys. Energy* **2020**, *2*, 032001.
- [20] J. Zhang, M.-R. Gao, J.-L. Luo, *Chem. Mater.* **2020**, *32*, 5424.
- [21] S. Singh, E. Prestat, L. F. Huang, J. M. Rondinelli, S. J. Haigh, B. A. Rosen, *Sci. Rep.* **2017**, *7*, 10080.
- [22] D. Neagu, V. Kyriakou, I.-L. Roiban, M. Aouine, C. Tang, A. Caravaca, K. Kousi, I. Schreur-Piet, I. S. Metcalfe, P. Vernoux, M. C. M. van de Sanden, M. N. Tsampas, *ACS Nano* **2019**, *13*, 12996.

- [23] Y. Gao, D. Chen, M. Saccoccio, Z. Lu, F. Ciucci, *Nano Energy* **2016**, 27, 499.
- [24] T.-S. Oh, E. K. Rahani, D. Neagu, J. T. S. Irvine, V. B. Shenoy, R. J. Gorte, J. M. Vohs, *J. Phys. Chem. Lett.* **2015**, 6, 5106.
- [25] M. B. Katz, S. Zhang, Y. Duan, H. Wang, M. Fang, K. Zhang, B. Li, G. W. Graham, X. Pan, *J. Catal.* **2012**, 293, 145.
- [26] D. Neagu, E. I. Papaioannou, W. K. W. Ramli, D. N. Miller, B. J. Murdoch, H. Ménard, A. Umar, A. J. Barlow, P. J. Cumpson, J. T. S. Irvine, I. S. Metcalfe, *Nat. Commun.* **2017**, 8, 1855.
- [27] H. Arandiyán, Y. Wang, J. Scott, S. Mesgari, H. Dai, R. Amal, *ACS Appl. Mater. Interfaces* **2018**, 10, 16352.
- [28] K. Kousi, D. Neagu, L. Bekris, E. Calì, G. Kerherve, E. I. Papaioannou, D. J. Payne, I. S. Metcalfe, *J. Mater. Chem. A* **2020**, 8, 12406.
- [29] T. Pussacq, O. Menétré, F. Tessier, A. Löfberg, M. Huvé, J. Guerro Caballero, S. Colis, H. Kabbour, *J. Alloys Compd.* **2018**, 766, 987.
- [30] V. B. Tinti, D. Marani, A. S. Ferlauto, F. C. Fonseca, V. Esposito, D. Z. de Florio, *Part. Part. Syst. Character.* **2020**, 37, 1900472.
- [31] A. R. West, *Solid State Chemistry and Its Applications*, 2nd ed., Wiley, Chichester, UK **2014**.
- [32] C. Yang, J. Li, Y. Lin, J. Liu, F. Chen, M. Liu, *Nano Energy* **2015**, 11, 704.
- [33] S.-K. Otto, K. Kousi, D. Neagu, L. Bekris, J. Janek, I. S. Metcalfe, *ACS Appl. Energy Mater.* **2019**, 2, 7288.
- [34] Y. Gao, Z. Lu, T. L. You, J. Wang, L. Xie, J. He, F. Ciucci, *J. Phys. Chem. Lett.* **2018**, 9, 3772.
- [35] F. N. Agüero, A. M. Beltrán, M. A. Fernández, L. E. Cadús, *J. Solid State Chem.* **2019**, 273, 75.
- [36] X. Mao, C. Lin, G. W. Graham, R. J. Gorte, *ACS Catal.* **2020**, 10, 8840.
- [37] C. Lin, A. C. Foucher, Y. Ji, C. D. Curran, E. A. Stach, S. McIntosh, R. J. Gorte, *ACS Catal.* **2019**, 9, 7318.
- [38] K. J. Kim, H. Han, T. Defferriere, D. Yoon, S. Na, S. J. Kim, A. M. Dayaghi, J. Son, T.-S. Oh, H. M. Jang, G. M. Choi, *J. Am. Chem. Soc.* **2019**, 141, 7509.
- [39] Y. Lu, Q. Shen, Q. Yu, F. Zhang, G. Li, W. Zhang, *J. Phys. Chem. C* **2016**, 120, 28712.
- [40] Z. Chen, B. Hua, X. Zhang, L. Chen, Y.-Q. Zhang, G. Yang, G. Wan, H. Zhou, Y. Yang, J. Chen, H. Fan, Q. Li, M. Li, J. Li, W. Zhou, Z. Shao, J.-L. Luo, Y. Sun, *Cell Rep. Phys. Sci.* **2020**, 1, 100243.
- [41] J. K. Kim, Y.-R. Jo, S. Kim, B. Koo, J. H. Kim, B.-J. Kim, W. Jung, *ACS Appl. Mater. Interfaces* **2020**, 12, 24039.
- [42] C. Tang, K. Kousi, D. Neagu, J. Portolés, E. I. Papaioannou, I. S. Metcalfe, *Nanoscale* **2019**, 11, 16935.
- [43] V. Kyriakou, D. Neagu, G. Zafeiropoulos, R. K. Sharma, C. Tang, K. Kousi, I. S. Metcalfe, M. C. M. van de Sanden, M. N. Tsampas, *ACS Catal.* **2019**, 10, 1278.
- [44] R. Thaling, M. Gocyla, M. Heggen, B. Klötzer, S. Penner, *J. Phys. Chem. C* **2015**, 119, 22050.
- [45] Y.-F. Sun, Y.-Q. Zhang, J. Chen, J.-H. Li, Y.-T. Zhu, Y.-M. Zeng, B. S. Amirkhiz, J. Li, B. Hua, J.-L. Luo, *Nano Lett.* **2016**, 16, 5303.
- [46] Z. Tian, K. Inagaki, Y. Morikawa, *Curr. Appl. Phys.* **2012**, 12, S105.
- [47] Y. Wang, X. Lei, Y. Zhang, F. Chen, T. Liu, *J. Power Sources* **2018**, 405, 114.
- [48] Z.-X. Tian, A. Uozumi, I. Hamada, S. Yanagisawa, H. Kizaki, K. Inagaki, Y. Morikawa, *Nanoscale Res. Lett.* **2013**, 8, 203.
- [49] S. Yanagisawa, A. Uozumi, I. Hamada, Y. Morikawa, *J. Phys. Chem. C* **2013**, 117, 1278.
- [50] H. Kizaki, H. Katayama-Yoshida, *Chem. Phys. Lett.* **2013**, 579, 85.
- [51] T. Jardiel, M. T. Caldes, F. Moser, J. Hamon, G. Gauthier, O. Joubert, *Solid State Ionics* **2010**, 181, 894.
- [52] K.-Y. Lai, A. Manthiram, *Chem. Mater.* **2018**, 30, 2515.
- [53] M. Shahid, P. Tiwari, S. Basu, *Ionics* **2019**, 25, 171.
- [54] S. Xu, D. Dong, Y. Wang, W. Doherty, K. Xie, Y. Wu, *J. Power Sources* **2014**, 246, 346.
- [55] C. Ni, Q. Zeng, D. He, L. Peng, D. Xie, J. T. S. Irvine, S. Duan, J. Ni, *J. Mater. Chem. A* **2019**, 7, 26944.
- [56] A. Eyssler, P. Mandaliev, A. Winkler, P. Hug, O. Safonova, R. Figi, A. Weidenkaff, D. Ferri, *J. Phys. Chem. C* **2010**, 114, 4584.
- [57] X. Zhang, H. Li, Y. Li, W. Shen, *Catal. Lett.* **2012**, 142, 118.
- [58] Y. Gao, J. Wang, Y.-Q. Lyu, K. Lam, F. Ciucci, *J. Mater. Chem. A* **2017**, 5, 6399.
- [59] S. Park, Y. Kim, Y. Noh, T. Kim, H. Han, W. Yoon, J. Choi, S.-H. Yi, W.-J. Lee, W. B. Kim, *J. Mater. Chem. A* **2020**, 8, 138.
- [60] A. Yaqub, N. K. Janjua, C. Savaniu, J. T. S. Irvine, *Int. J. Hydrogen Energy* **2015**, 40, 760.
- [61] O. Kwon, S. Sengodan, K. Kim, G. Kim, H. Y. Jeong, J. Shin, Y.-W. Ju, J. W. Han, G. Kim, *Nat. Commun.* **2017**, 8, 15967.
- [62] Y. Sun, J. Li, Y. Zeng, B. S. Amirkhiz, M. Wang, Y. Behnamian, J. Luo, *J. Mater. Chem. A* **2015**, 3, 11048.
- [63] Z. Du, H. Zhao, S. Yi, Q. Xia, Y. Gong, Y. Zhang, X. Cheng, Y. Li, L. Gu, K. Świerczek, *ACS Nano* **2016**, 10, 8660.
- [64] Y. Wang, T. Liu, M. Li, C. Xia, B. Zhou, F. Chen, *J. Mater. Chem. A* **2016**, 4, 14163.
- [65] Y.-F. Sun, Y.-L. Yang, J. Chen, M. Li, Y.-Q. Zhang, J.-H. Li, B. Hua, J.-L. Luo, *Chem. Commun.* **2018**, 54, 1505.
- [66] B. Yan, Q. Wu, J. Cen, J. Timoshenko, A. I. Frenkel, D. Su, X. Chen, J. B. Parise, E. Stach, A. Orlov, J. G. Chen, *Appl. Catal., B* **2018**, 237, 1003.
- [67] O. Ben Mya, L. dos Santos-Gómez, J. M. Porras-Vázquez, M. Omari, J. R. Ramos-Barrado, D. Marrero-López, *Int. J. Hydrogen Energy* **2017**, 42, 23160.
- [68] S. Song, J. Zhou, X. Su, Y. Wang, J. Li, L. Zhang, G. Xiao, C. Guan, R. Liu, S. Chen, H.-J. Lin, S. Zhang, J.-Q. Wang, *Energy Environ. Sci.* **2018**, 11, 2945.
- [69] Y.-Q. Zhang, H.-B. Tao, J. Liu, Y.-F. Sun, J. Chen, B. Hua, T. Thundat, J.-L. Luo, *Nano Energy* **2017**, 38, 392.
- [70] J. Bian, Z. Li, N. Li, C. Sun, *Inorg. Chem.* **2019**, 58, 8208.
- [71] Y.-F. Sun, Y.-Q. Zhang, Y.-L. Yang, J. Chen, B. Hua, Y.-X. Shi, C.-A. Wang, J.-L. Luo, *Appl. Catal., B* **2017**, 219, 640.
- [72] Y.-R. Jo, B. Koo, M.-J. Seo, J. K. Kim, S. Lee, K. Kim, J. W. Han, W. Jung, B.-J. Kim, *J. Am. Chem. Soc.* **2019**, 141, 6690.
- [73] M. van den Bossche, S. McIntosh, *Chem. Mater.* **2010**, 22, 5856.
- [74] T.-S. Oh, A. S. Yu, L. Adjianto, R. J. Gorte, J. M. Vohs, *J. Power Sources* **2014**, 262, 207.
- [75] S. Vecino-Mantilla, P. Gauthier-Maradei, M. Huvé, J. M. Serra, P. Roussel, G. H. Gauthier, *ChemCatChem* **2019**, 11, 4631.
- [76] Y.-F. Sun, X.-W. Zhou, Y. Zeng, B. S. Amirkhiz, M.-N. Wang, L.-Z. Zhang, B. Hua, J. Li, J.-H. Li, J.-L. Luo, *J. Mater. Chem. A* **2015**, 3, 22830.
- [77] W. Qi, K. Xie, M. Liu, G. Wu, Y. Wang, Y. Zhang, Y. Wu, *RSC Adv.* **2014**, 4, 40494.
- [78] L. Ye, M. Zhang, P. Huang, G. Guo, M. Hong, C. Li, J. T. S. Irvine, K. Xie, *Nat. Commun.* **2017**, 8, 14785.
- [79] C. Duan, R. J. Kee, H. Zhu, C. Karakaya, Y. Chen, S. Ricote, A. Jarry, E. J. Crumlin, D. Hook, R. Braun, N. P. Sullivan, R. O'Hayre, *Nature* **2018**, 557, 217.
- [80] J. Tan, D. Lee, J. Ahn, B. Kim, J. Kim, J. Moon, *J. Mater. Chem. A* **2018**, 6, 18133.
- [81] Y. Song, W. Wang, L. Ge, X. Xu, Z. Zhang, P. S. B. Julião, W. Zhou, Z. Shao, *Adv. Sci.* **2017**, 4, 1700337.
- [82] Y. Song, H. Li, M. Xu, G. Yang, W. Wang, R. Ran, W. Zhou, Z. Shao, *Small* **2020**, 16, 2001859.
- [83] T. Zhu, H. Troiani, L. V. Mogni, M. Santaya, M. Han, S. A. Barnett, *J. Power Sources* **2019**, 439, 227077.
- [84] J. Feng, J. Qiao, W. Wang, Z. Wang, W. Sun, K. Sun, *Electrochim. Acta* **2016**, 215, 592.
- [85] K. J. Kim, M. K. Rath, H. H. Kwak, H. J. Kim, J. W. Han, S.-T. Hong, K. T. Lee, *ACS Catal.* **2019**, 9, 1172.
- [86] Z. Xu, Y. Li, Y. Wan, S. Zhang, C. Xia, *J. Power Sources* **2019**, 425, 153.
- [87] C. Arrivé, T. Delahaye, O. Joubert, G. H. Gauthier, *Ceram. Int.* **2020**, 46, 5841.

- [88] J. Zhang, K. Xie, Y. Gan, G. Wu, B. Ding, Y. Zhang, Y. Wu, *New J. Chem.* **2014**, *38*, 3434.
- [89] L. Yang, K. Xie, S. Xu, T. Wu, Q. Zhou, T. Xie, Y. Wu, *Dalton Trans.* **2014**, *43*, 14147.
- [90] G. Tsekouras, D. Neagu, J. T. S. Irvine, *Energy Environ. Sci.* **2013**, *6*, 256.
- [91] Y. Zhu, J. Dai, W. Zhou, Y. Zhong, H. Wang, Z. Shao, *J. Mater. Chem. A* **2018**, *6*, 13582.
- [92] H. Wei, K. Xie, J. Zhang, Y. Zhang, Y. Wang, Y. Qin, J. Cui, J. Yan, Y. Wu, *Sci. Rep.* **2014**, *4*, 5156.
- [93] L. Yang, X. Xue, K. Xie, *Phys. Chem. Chem. Phys.* **2015**, *17*, 11705.
- [94] V. Kyriakou, D. Neagu, E. I. Papaioannou, I. S. Metcalfe, M. C. M. van de Sanden, M. N. Tsampas, *Appl. Catal., B* **2019**, *258*, 117950.
- [95] P. Steiger, O. Kröcher, D. Ferri, *Appl. Catal., A* **2020**, *590*, 117328.
- [96] J. Deng, M. Cai, W. Sun, X. Liao, W. Chu, X. S. Zhao, *ChemSusChem* **2013**, *6*, 2061.
- [97] Y. S. Park, M. Kang, P. Byeon, S.-Y. Chung, T. Nakayama, T. Ko, H. Hwang, *J. Power Sources* **2018**, *397*, 318.
- [98] P. Littlewood, X. Xie, M. Bernicke, A. Thomas, R. Schomäcker, *Catal. Today* **2015**, *242*, 111.
- [99] S. P. Padi, L. Shelly, E. P. Komarala, D. Schweke, S. Hayun, B. A. Rosen, *Catal. Commun.* **2020**, *138*, 105951.
- [100] R. Thalinger, M. Gocyla, M. Heggen, R. Dunin-Borkowski, M. Grünbacher, M. Stöger-Pollach, D. Schmidmair, B. Klötzer, S. Penner, *J. Catal.* **2016**, *337*, 26.
- [101] S. Q. Chen, Y. D. Li, Y. Liu, X. Bai, *Int. J. Hydrogen Energy* **2011**, *36*, 5849.
- [102] X. Yang, T. Wei, B. Chi, J. Pu, J. Li, *J. Catal.* **2019**, *377*, 629.
- [103] D. Papargyriou, J. T. S. Irvine, *Solid State Ionics* **2016**, *288*, 120.
- [104] G. Dimitrakopoulos, A. F. Ghoniem, B. Yildiz, *Sustainable Energy Fuels* **2019**, *3*, 2347.
- [105] J. Li, B. Wei, X. Yue, H. Li, Z. Lü, *Electrochim. Acta* **2019**, *304*, 30.
- [106] S. Hou, K. Xie, *Electrochim. Acta* **2019**, *301*, 63.
- [107] H. Qi, F. Xia, T. Yang, W. Li, W. Li, L. Ma, G. Collins, W. Shi, H. Tian, S. Hu, T. Thomas, E. M. Sabolsky, J. Zondlo, R. Hart, H. Finklea, G. A. Hackett, X. Liu, *J. Electrochem. Soc.* **2020**, *167*, 024510.
- [108] H. Lv, L. Lin, X. Zhang, D. Gao, Y. Song, Y. Zhou, Q. Liu, G. Wang, X. Bao, *J. Mater. Chem. A* **2019**, *7*, 11967.
- [109] S. Kralj, F. Longobardo, D. Iglesias, M. Bevilacqua, C. Tavagnacco, A. Criado, J. J. Delgado Jaen, D. Makovec, S. Marchesan, M. Melchionna, M. Prato, P. Fornasiero, *ACS Appl. Nano Mater.* **2019**, *2*, 6092.
- [110] W. Ng, Y. Yang, K. van der Veen, G. Rothenberg, N. Yan, *Carbon* **2018**, *129*, 293.
- [111] H. Lv, L. Lin, X. Zhang, Y. Song, H. Matsumoto, C. Zeng, N. Ta, W. Liu, D. Gao, G. Wang, X. Bao, *Adv. Mater.* **2020**, *32*, 1906193.
- [112] L. Gan, L. Ye, C. Ruan, S. Chen, K. Xie, *Adv. Sci.* **2016**, *3*, 1500186.
- [113] A. K. Opitz, A. Nanning, C. Rameshan, R. Rameshan, R. Blume, M. Hävecker, A. Knop-Gericke, G. Rupprechter, J. Fleig, B. Klötzer, *Angew. Chem., Int. Ed.* **2015**, *54*, 2628.
- [114] A. Nanning, J. Fleig, *Surf. Sci.* **2019**, *680*, 43.
- [115] S. Liu, W. Zhang, T. Deng, D. Wang, X. Wang, X. Zhang, C. Zhang, W. Zheng, *ChemCatChem* **2017**, *9*, 3102.
- [116] F. Fang, N. Feng, P. Zhao, C. Chen, X. Li, J. Meng, G. Liu, L. Chen, H. Wan, G. Guan, *Chem. Eng. J.* **2019**, *372*, 752.
- [117] A. J. Carrillo, K. J. Kim, Z. D. Hood, A. H. Bork, J. L. M. Rupp, *ACS Appl. Energy Mater.* **2020**, *3*, 4569.
- [118] S. Liu, Q. Liu, X.-Z. Fu, J.-L. Luo, *Appl. Catal., B* **2018**, *220*, 283.
- [119] Y. Yang, Y. Wang, Z. Yang, Z. Lei, C. Jin, Y. Liu, Y. Wang, S. Peng, *J. Power Sources* **2019**, *438*, 226989.
- [120] F. Lu, T. Xia, Q. Li, J. Wang, L. Huo, H. Zhao, *Appl. Catal., B* **2019**, *249*, 19.
- [121] J. Zhou, T.-H. Shin, C. Ni, G. Chen, K. Wu, Y. Cheng, J. T. S. Irvine, *Chem. Mater.* **2016**, *28*, 2981.
- [122] Y.-Q. Zhang, H.-B. Tao, Z. Chen, M. Li, Y.-F. Sun, B. Hua, J.-L. Luo, *J. Mater. Chem. A* **2019**, *7*, 26607.
- [123] Y.-F. Sun, J.-H. Li, Y.-Q. Zhang, B. Hua, J.-L. Luo, *ACS Catal.* **2016**, *6*, 2710.
- [124] N. Escalona, S. Fuentealba, G. Pecchi, *Appl. Catal., A* **2010**, *381*, 253.
- [125] S. Joo, O. Kwon, K. Kim, S. Kim, H. Kim, J. Shin, H. Y. Jeong, S. Sengodan, J. W. Han, G. Kim, *Nat. Commun.* **2019**, *10*, 697.
- [126] H. Li, G. Sun, K. Xie, W. Qi, Q. Qin, H. Wei, S. Chen, Y. Wang, Y. Zhang, Y. Wu, *Int. J. Hydrogen Energy* **2014**, *39*, 20888.
- [127] W. Qi, C. Ruan, G. Wu, Y. Zhang, Y. Wang, K. Xie, Y. Wu, *Int. J. Hydrogen Energy* **2014**, *39*, 5485.
- [128] N. Zhou, Y.-M. Yin, Z. Chen, Y. Song, J. Yin, D. Zhou, Z.-F. Ma, *J. Electrochem. Soc.* **2018**, *165*, F629.
- [129] D. Hosseini, F. Donat, P. M. Abdala, S. M. Kim, A. M. Kierzkowska, C. R. Müller, *ACS Appl. Mater. Interfaces* **2019**, *11*, 18276.
- [130] S. Sengodan, Y.-W. Ju, O. Kwon, A. Jun, H. Y. Jeong, T. Ishihara, J. Shin, G. Kim, *ACS Sustainable Chem. Eng.* **2017**, *5*, 9207.
- [131] P. Xiao, X. Ge, Z. Liu, J.-Y. Wang, X. Wang, *J. Alloys Compd.* **2014**, *587*, 326.
- [132] L. Ye, C. Pan, M. Zhang, C. Li, F. Chen, L. Gan, K. Xie, *ACS Appl. Mater. Interfaces* **2017**, *9*, 25350.
- [133] Y. Chen, Y. Chen, D. Ding, Y. Ding, Y. Choi, L. Zhang, S. Yoo, D. Chen, B. deGlee, H. Xu, Q. Lu, B. Zhao, G. Vardar, J. Wang, H. Bluhm, E. J. Crumlin, C. Yang, J. Liu, B. Yildiz, M. Liu, *Energy Environ. Sci.* **2017**, *10*, 964.
- [134] A. Eysler, E. Kleymenov, A. Kupferschmid, M. Nachtegaal, M. S. Kumar, P. Hug, A. Weidenkaff, D. Ferri, *J. Phys. Chem. C* **2011**, *115*, 1231.
- [135] X. Li, C. Chen, C. Liu, H. Xian, L. Guo, J. Lv, Z. Jiang, P. Vernoux, *ACS Catal.* **2013**, *3*, 1071.
- [136] M. Kurnatowska, L. Kepinski, W. Mista, *Appl. Catal., B* **2012**, *117–118*, 135.
- [137] X. Li, L. Dai, Z. He, W. Meng, Y. Li, L. Wang, *Sens. Actuators, B* **2019**, *298*, 126827.
- [138] T. H. Shin, Y. Okamoto, S. Ida, T. Ishihara, *Chem. - Eur. J.* **2012**, *18*, 11695.
- [139] K. Chen, S. He, N. Li, Y. Cheng, N. Ai, M. Chen, W. D. A. Rickard, T. Zhang, S. P. Jiang, *J. Power Sources* **2018**, *378*, 433.
- [140] H. Tanaka, M. Taniguchi, M. Uenishi, N. Kajita, I. Tan, Y. Nishihata, J. Mizuki, K. Narita, M. Kimura, K. Kaneko, *Angew. Chem., Int. Ed.* **2006**, *45*, 5998.
- [141] G. C. Mondragón Rodríguez, Y. Gönüllü, B. Saruhan, *Top. Catal.* **2013**, *56*, 397.
- [142] Q. Wu, B. Yan, J. Cen, J. Timoshenko, D. N. Zakharov, X. Chen, H. L. Xin, S. Yao, J. B. Parise, A. I. Frenkel, E. A. Stach, J. G. Chen, A. Orlov, *Chem. Mater.* **2018**, *30*, 1585.
- [143] F. Kosaka, N. Noda, T. Nakamura, J. Otomo, *J. Mater. Sci.* **2017**, *52*, 2825.
- [144] N. K. Monteiro, F. B. Noronha, L. O. O. da Costa, M. Linardi, F. C. Fonseca, *Int. J. Hydrogen Energy* **2012**, *37*, 9816.
- [145] Y. Jiang, Z. Geng, L. Yuan, Y. Sun, Y. Cong, K. Huang, L. Wang, W. Zhang, *ACS Sustainable Chem. Eng.* **2018**, *6*, 11999.
- [146] J. Zhou, N. Wang, J. Cui, J. Wang, J. Yang, Z. Zong, Z. Zhang, Q. Chen, X. Zheng, K. Wu, *J. Alloys Compd.* **2019**, *792*, 1132.
- [147] G. S. Kim, B. Y. Lee, H. C. Ham, J. Han, S. W. Nam, J. Moon, S. P. Yoon, *Int. J. Hydrogen Energy* **2019**, *44*, 202.
- [148] M. A. Naeem, P. M. Abdala, A. Armutlulu, S. M. Kim, A. Fedorov, C. R. Müller, *ACS Catal.* **2020**, *10*, 1923.
- [149] X. Xu, G. Liu, A. K. Azad, *Int. J. Hydrogen Energy* **2015**, *40*, 3672.
- [150] J. Yu, L. Zhang, J. Qian, Z. Zhu, S. Ni, G. Liu, X. Xu, *Appl. Catal., B* **2019**, *256*, 117818.

- [151] M. Xu, W. Wang, Y. Zhong, X. Xu, J. Wang, W. Zhou, Z. Shao, *J. Mater. Chem. A* **2019**, *7*, 17489.
- [152] R. Sažinas, K. B. Andersen, K. K. Hansen, *J. Solid State Electrochem.* **2020**, *24*, 609.
- [153] J. H. Kim, J. K. Kim, H. G. Seo, D.-K. Lim, S. J. Jeong, J. Seo, J. Kim, W. Jung, *Adv. Funct. Mater.* **2020**, *30*, 2001326.
- [154] X. Li, L. Dai, Z. He, W. Meng, Y. Li, L. Wang, *Sens. Actuators, B* **2019**, *298*, 126854.
- [155] J. H. Oh, B. W. Kwon, J. Cho, C. H. Lee, M. K. Kim, S. H. Choi, S. P. Yoon, J. Han, S. W. Nam, J. Y. Kim, S. S. Jang, K. B. Lee, H. C. Ham, *Ind. Eng. Chem. Res.* **2019**, *58*, 6385.
- [156] E. Cali, G. Kerherve, F. Naufal, K. Kousi, D. Neagu, E. I. Papaioannou, M. P. Thomas, B. S. Gupton, I. S. Metcalfe, J. T. S. Irvine, D. J. Payne, *ACS Appl. Mater. Interfaces* **2020**, *12*, 37444.
- [157] J.-S. Jang, J. K. Kim, K. Kim, W.-G. Jung, C. Lim, S. Kim, D.-H. Kim, B.-J. Kim, J. W. Han, W. Jung, I.-D. Kim, *Adv. Mater.* **2020**, *32*, 2003983.
- [158] E. le Saché, L. Pastor-Pérez, D. Watson, A. Sepúlveda-Escribano, T. R. Reina, *Appl. Catal., B* **2018**, *236*, 458.
- [159] Y. Chen, Y. Zhang, G. Xiao, Z. Yang, M. Han, F. Chen, *ChemElectroChem* **2015**, *2*, 672.
- [160] Y. Li, B. Hu, C. Xia, W. Q. Xu, J. P. Lemmon, F. Chen, *J. Mater. Chem. A* **2017**, *5*, 20833.
- [161] S. Kumar, R. Parthasarathy, A. P. Singh, B. Wickman, M. Thirumal, A. K. Ganguli, *Catal. Sci. Technol.* **2017**, *7*, 481.
- [162] H. Khalid, A. U. Haq, C. Savaniu, J. T. S. Irvine, D. Mariotti, *ECS Meet. Abstr.* **2020**, *MA2020-01*, 1123.
- [163] T. Götsch, L. Schlicker, M. F. Bekheet, A. Doran, M. Grünbacher, C. Praty, M. Tada, H. Matsui, N. Ishiguro, A. Gurlo, B. Klötzer, S. Penner, *RSC Adv.* **2018**, *8*, 3120.



Kalliopi Kousi received her degree in chemistry from the University of Patras, Greece, in 2011. She has an M.Res. (2013) and a Ph.D. (2016) on “Catalysis for Environmental Protection and Clean Energy Production” and has worked as postdoctoral research associate at the Department of Chemical Engineering focusing on catalysts for LPG conversion. She joined the Application of Ion Transport Group at Newcastle University as a postdoctoral research associate in 2017. Her research interest lies in new materials and structures for different catalytic applications, currently focusing on emergent nanomaterials for energy conversion processes.



Ian S. Metcalfe obtained his first degree in chemical engineering from the Imperial College and then studied at Princeton University. He is currently a professor of chemical engineering at Newcastle University. Ian is a fellow of the Institution of Chemical Engineers and a fellow of the Royal Society of Chemistry. He was elected a fellow of the Royal Academy of Engineering (RAEng) in 2012. He currently holds an RAEng Chair in Emerging Technologies. His research concerns the thermodynamics of chemical conversion with an emphasis on energy processes. He has a particular interest in membrane processes, solid–gas reactions, and solid state chemistry.



Dragos Neagu obtained his degree in chemical engineering from University Politehnica of Bucharest, Romania, in 2008. He received his Ph.D. on materials and devices for electrochemical energy conversion from the University of St. Andrews, UK, in 2013. He then worked as a postdoctoral researcher at the University of St. Andrews and Newcastle University. In 2020, he joined the University of Strathclyde as a lecturer in the Department of Chemical and Process Engineering. His research interests are in the design, preparation, multiscale characterization, and application of nanostructured, functional materials for renewable energy conversion technologies.